A Silurian–Devonian marine platform-deltaic system in the San Rafael Block, Argentine Precordillera–Cuyania terrane: lithofacies and provenance

M. J. MANASSERO[1]*, C. A. CINGOLANI[1,2] & P. ABRE[2]

[1]*Centro de Investigaciones Geológicas (UNLP-CONICET), Facultad de Ciencias Naturales y Museo, Universidad Nacional de La Plata, 1-644, (1900)-La Plata, Argentina*

[2]*División Científica de Geología-Facultad Ciencias Naturales y Museo, Universidad Nacional de La Plata, Paseo del Bosque s/n, (1900)-La Plata, Argentina*

**Corresponding author (e-mail: manasser@cig.museo.unlp.edu.ar)*

Abstract: The San Rafael Block is included as a part of the pre-Andean region, in the southern sector of the Argentine Precordillera–Cuyania terrane, within the western Gondwana margin. The Río Seco de los Castaños Formation (Upper Silurian–Lower Devonian) is one of the major marine-siliciclastic pre-Carboniferous units, and is interpreted as a distal to proximal silty platform-deltaic system. The dominant sedimentary processes were wave and storm action and the source areas were located to the east, close to the study area. The rocks are mainly of immature arkosic sandstones showing both recycled orogen and continental block provenances. Sedimentological characteristics of conglomerate-filled channels and an organic-matter-rich bed are described. X-ray diffraction analyses of the clay minerals from the sequences show that very low-grade metamorphic conditions acted during the Early Carboniferous. Geochemical analyses indicate moderate to strong weathering, and potassium metasomatism. Zr/Sc ratios lower than 22, no important enrichments of Zr, Th/Sc ratios, high Sc and Cr concentration and the Eu-anomalies indicate a provenance from a less evolved upper continental crust. T_{DM} ages and ε_{Nd} are within the range of the Mesoproterozoic basement and Palaeozoic supracrustal rocks from the Precordillera–Cuyania terrane. Probable sources, tectonic setting and land–sea interactions are discussed.

The southern Pacific South America Gondwana margin (Fig. 1a) is characterized during the Palaeozoic by the presence of orogenic belts orientated approximately north–south (Ramos *et al.* 1986). They were accreted to the cratonic areas during the Cambrian (Pampean), Mid-Ordovician (Famatinian) and Late Devonian (Gondwanian) tectonic cycles (Fig. 1b). The Argentine Precordillera or Cuyania composite terrane in the sense of Ramos *et al.* (1986) is related to the Famatinian cycle and lies eastward of the present-day Andes. Four sectors constitute this composite terrane: (a) the Precordillera thin-skinned fold and thrust belt that was generated by shallow east-dipping flat-slab subduction of the Nazca plate; (b) the Pie de Palo area, (c) San Rafael and (d) Las Matras blocks. This terrane had been considered stratigraphically and faunally unique to South America mainly for the Lower Palaeozoic carbonate and siliciclastic deposits overlying an igneous-metamorphic crust of 'Grenville age' (Ramos *et al.* 1998; Sato *et al.* 2004, and references therein). The Precordillera–Cuyania terrane has been the object of several lines of research during recent years, attempting to constrain its allochthonous or para-autochthonous origin with respect to Gondwana. One of the tectonic interpretations suggests that the Precordillera–Cuyania was detached from Laurentia in Cambrian times, was transferred to western Gondwana during the Early to Middle Ordovician, and was amalgamated to the early proto-Andean margin of Gondwana by the Mid-Late Ordovician (Thomas & Astini 2003 and references therein). Other studies have claimed a para-autochthonous-to-Gondwana origin based on strike-slip displacements from the South Africa–Antarctica regions (Aceñolaza *et al.* 2002; Finney *et al.* 2003). A late Middle to Late Ordovician time of docking for the Precordillera–Cuyania is constrained by a variety of geological and palaeontological evidence (Ramos 2004 and references therein). The terrane deformation linked to the collision started in the Ordovician, and continued until the time of approach of the Chilenia terrane during the Late Devonian, against the Pacific side (Fig. 1b).

In this tectonic scenario, Silurian–Devonian siliciclastic depocentres of foreland basins were developed in the Precordillera–Cuyania terrane. One of them is preserved in the San Rafael Block, within the southern sector of this terrane (Fig. 2).

From: KÖNIGSHOF, P. (ed.) *Devonian Change: Case Studies in Palaeogeography and Palaeoecology*. The Geological Society, London, Special Publications, **314**, 213–238.
DOI: 10.1144/SP314.12 0305-8719/09/$15.00 © The Geological Society of London 2009.

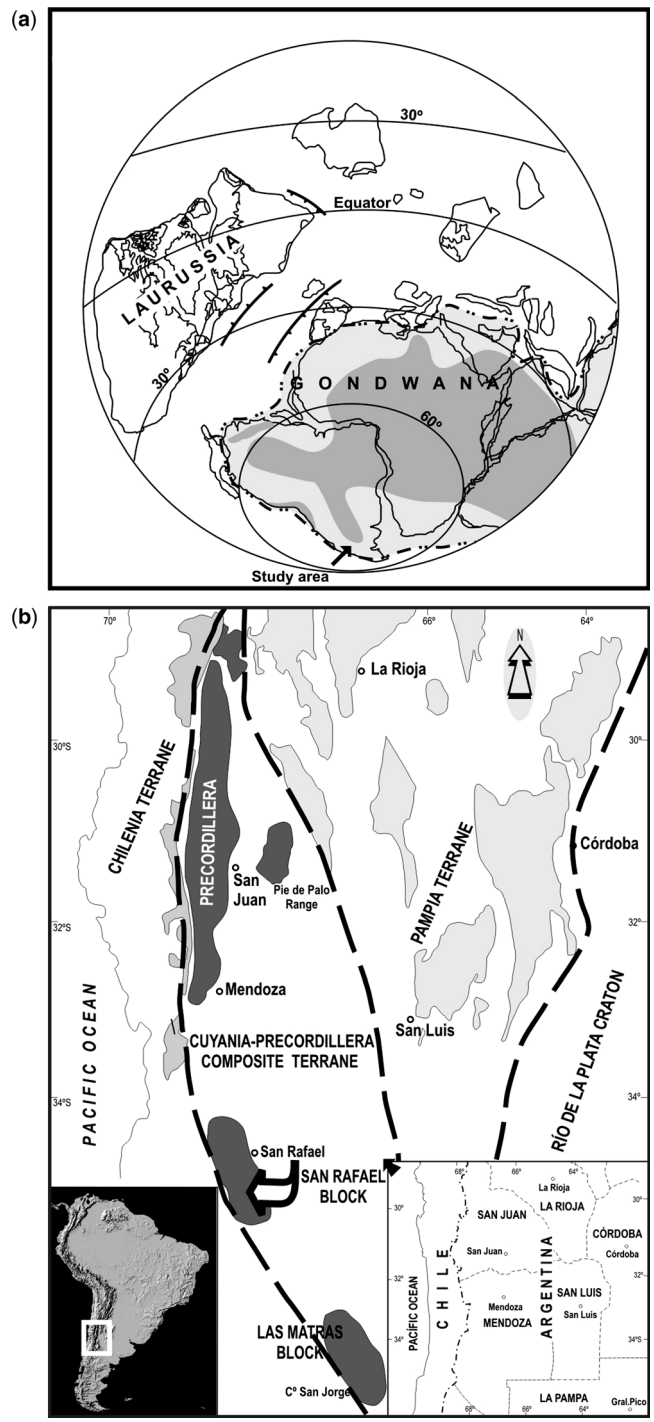

Fig. 1. (**a**) Location of the San Rafael Block in the Upper Silurian–Lower Devonian palaeogeographic reconstruction (after Torsvik & Cocks 2004). In Gondwana continent land masses are dark grey, marine transgressions are grey. (**b**) Regional location map showing the pre-Andean San Rafael Block in the Argentine Precordillera–Cuyania composite terrane and arrangement of the adjacent tectonic terranes.

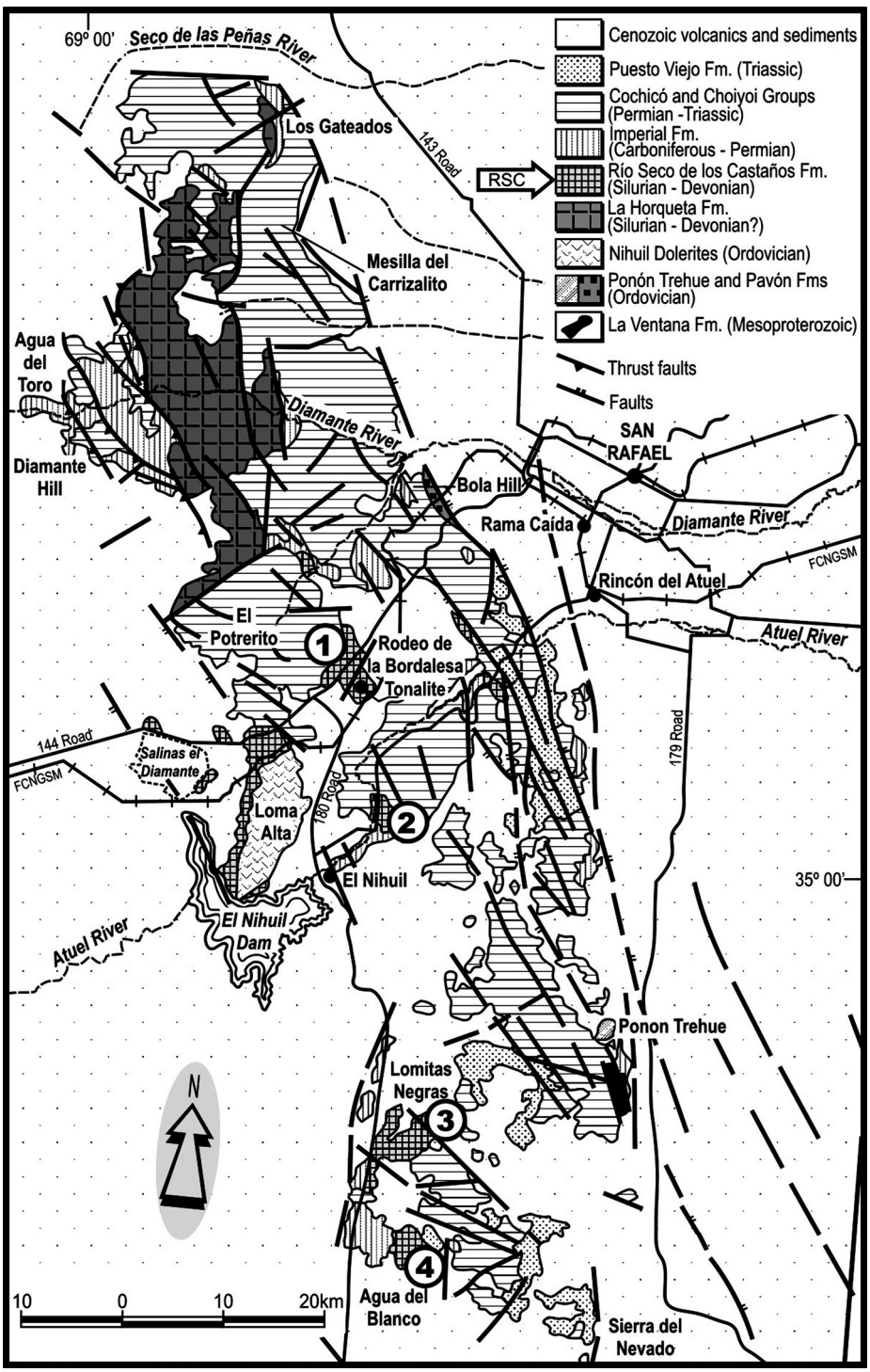

Fig. 2. Geological sketch map of the NW–SE trending San Rafael Block (simplified from Dessanti 1956; González Díaz 1972; Nuñez 1976). Main outcrops of the Río Seco de los Castaños Formation mentioned in text: 1, Road 144–Rodeo Bordalesa; 2, Atuel creek (type section); 3, Lomitas Negras; and 4, Agua del Blanco sections.

The San Rafael Block is a NW–SE trending morpho-structural entity located in the south-central part of the Mendoza Province, Argentina. It is mainly composed of isolated outcrops of 'pre-Carboniferous units' (Mesoproterozoic to Devonian in age), Upper Palaeozoic sedimentary and volcaniclastic rocks, Permian–Triassic volcaniclastic and magmatic complexes and an extended Cenozoic volcanism. In an integrated lithostratigraphic column (Fig. 3) the stratigraphic sequence, relationships, rock types and ages of the different units that composed the San Rafael Block are summarized. The Río Seco de los Castaños Formation (González Díaz 1972, 1981) is one of the above-mentioned 'pre-Carboniferous units'. Based on the stratigraphical and palaeontological evidence, the age of the unit is constrained to between the Late Silurian and Early Devonian.

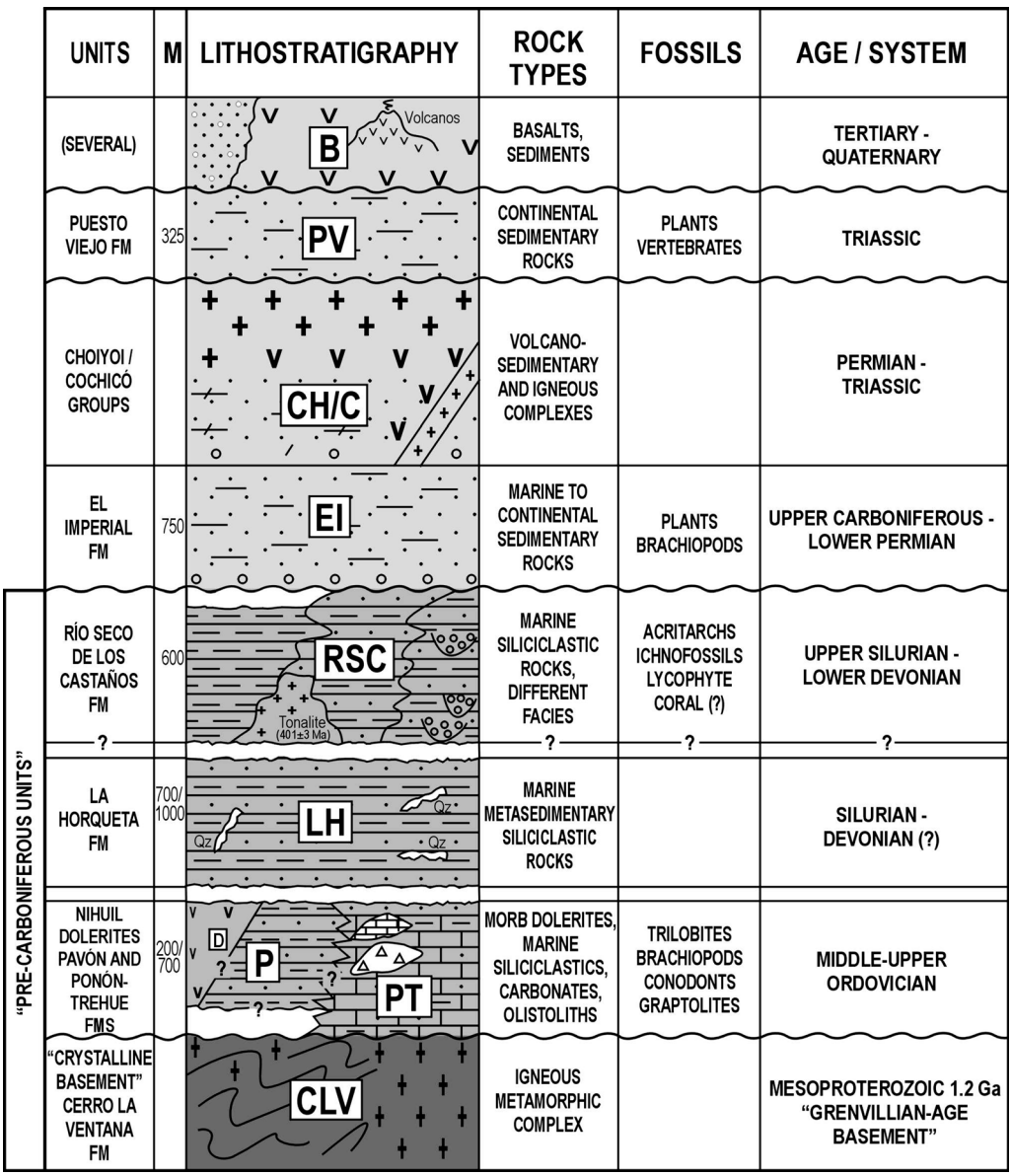

Fig. 3. Integrated lithostratigraphic column-chart from the San Rafael Block. Note that the Río Seco de los Castaños Formation is the youngest of the 'pre-Carboniferous units'.

The focus of this paper is to describe and integrate the sedimentology, mineral composition, geochemistry and isotope data of the Río Seco de los Castaños unit. The combination of these different approaches can reveal the provenance and nature of the source areas and the tectonic setting of the sedimentary basin. At the same time, this study has yielded valuable insights into the crustal processes evolving land–sea interactions during Silurian–Devonian times at the San Rafael Block.

Geological setting

The Río Seco de los Castaños Formation was included in La Horqueta, a low grade metamorphic unit (Dessanti 1956), from which it was later differentiated based on its sedimentary characteristics by González Díaz (1981). The Río Seco de los Castaños Formation was assigned to the Devonian by Di Persia (1972), due to the presence of corals similar to *Pleurodyctium*. Contributions by Nuñez (1976) and Criado Roque & Ibañez (1979) described other sedimentary features of this foreland marine sequence. Poiré *et al.* (2002) recognized some trace fossil associations that helped to interpret different subenvironments of deposition within a wide siliciclastic marine platform. Neither the base nor the top of the Río Seco de los Castaños Formation are exposed. It is separated from the Carboniferous–Lower Permian El Imperial Formation (a fossiliferous marine/continental sedimentary unit) by an angular unconformity. During the Permian and Triassic, magmatic rocks and thick volcaniclastic complexes of the Cochicó-Choiyoy Groups were developed in the San Rafael Block (Fig. 3).

The main outcrops of the unit (which were dismembered by Mesozoic and Cenozoic tectonism) are rather isolated within the San Rafael Block and, as suggested by Cuerda & Cingolani (1998) and Cingolani *et al.* (2003*b*), they are located at the following sections (Fig. 2).

(a) *Road 144–Rodeo de la Bordalesa*. Outcrops where Rubinstein (1997) found acritarchs and other microfossils assigned to the Upper Silurian. Trace fossils such as the *Nereites–Mermia facies* were mentioned by some authors (Criado Roque & Ibañez 1979; Poiré *et al.* 2003). The tonalite body intruded into the Río Seco de los Castaños Formation, shows U–Pb (in zircons) and K–Ar (in biotite) crystallization ages of 401 ± 3 Ma (Lower Devonian; Cingolani *et al.* 2003*a*), which also constrain the sedimentation age of the Río Seco de los Castaños Formation.

(b) *Atuel Creek* (Figs 4 and 5). The type-section of the sequence (González Díaz 1981) is located in this creek. The two main outcrops are present about 12 km NE of El Nihuil town and near the Valle Grande dam. The Río Seco de los Castaños Formation comprises here about 600 m of tabular, green sandstones and mudstones with sharp contacts. This unit has regional folding and dips 50–72° to the SE or NE. Upper Palaeozoic horizontally bedded sedimentary rocks are found above the Río Seco de los Castaños Formation, displaying a notable angular unconformity with the Río Seco de los Castaños Formation (Fig. 4a). In the Atuel Creek area fragments

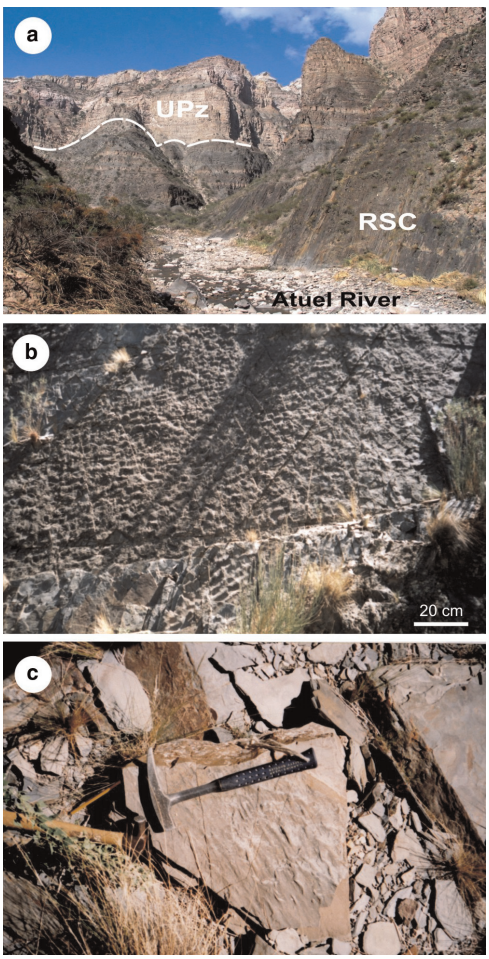

Colour online

Fig. 4. (**a**) Panoramic view at the Atuel creek type section. The angular unconformity between the Río Seco de los Castaños Formation (RSC) and the Upper Palaeozoic sedimentary units (UPz) is shown. (**b**) Current and wave ripples at the top of sandstone beds (middle section). (**c**) Substratal sedimentary structures at the base of massive sandstones.

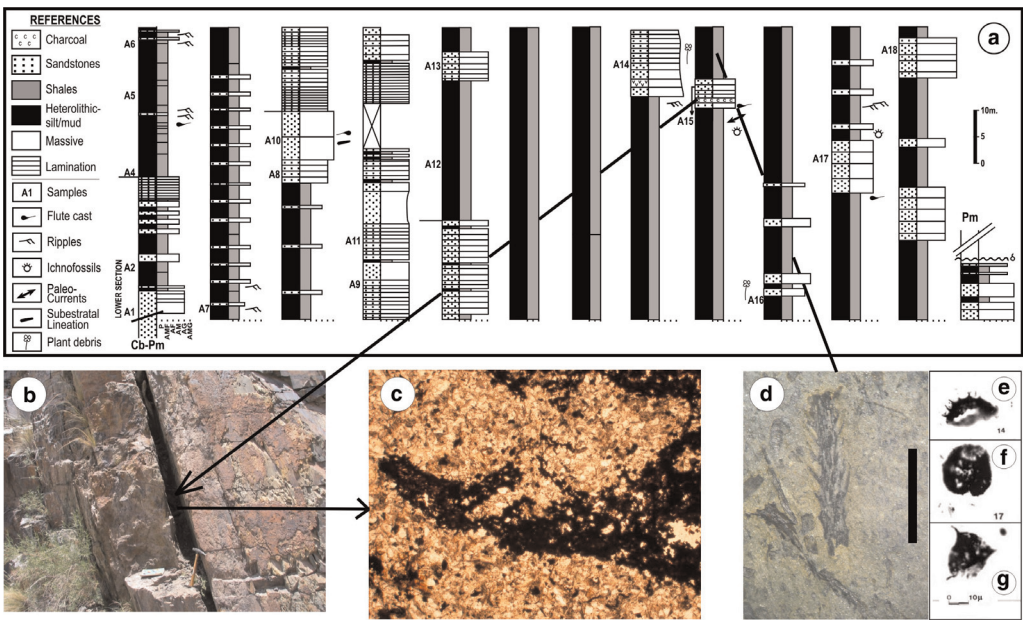

Colour online

Fig. 5. (**a**) Sedimentary log of the Atuel creek section, with details of lithology and structures. (**b**) Charcoal bed field photograph and (**c**) photomicrograph detail showing the silty-quartz material (light colour) and the relicts of organic matter in black. (**d**) Detail of the fossil plants *Lycophytes* sp. (after Morel *et al.* 2006) black bar = 1 cm. (**e**) Microphotograph of spores and acritarchs (after Pöthe de Baldis, unpubl. data); (**f**) *Ammonidium* sp.; (**g**) *Lophosphaeridium* sp.

of fossil plants such as *Lycophytes* (Fig. 5d) are described and assigned to the Lower Devonian (Morel *et al.* 2006). Marine microfossils such as prasinophytes, spores and acritarchs were found by Pöthe de Baldis unpubl. data indicating shallow water conditions near the coastline and suggesting an Upper Silurian age (Fig. 5e, f and g).

(c) *Nihuil area*. The sequence assigned to the Río Seco de los Castaños Formation is overlying the Ordovician MORB-type dolerite rocks called 'El Nihuil mafic body' at the Loma Alta region (Cingolani *et al.* 2003*b*).

(d) *Lomitas Negras* (Fig. 6) *and Agua del Blanco* (Fig. 7) *areas*. The studied unit includes here the southernmost outcrops, where Di Persia (1972) mentioned a coral of Devonian age and conglomerates with limestone clasts bearing Ordovician fossils.

Methods

Sedimentology

During fieldwork, measurements and descriptions were made of several sedimentological sections and detailed sampling of all the lithological types was undertaken (Manassero *et al.* 2005). Thin sections were examined using optical microscopy to determine the textural and optical properties of minerals as well as paragenetic associations. Selected samples were tinted with alizarine red to determine feldspars under the optical microscope. Scanning electron microscopy (SEM) was used to examine textural features, mineral morphology and the diagenetic sequence of formation. The samples were collected along Road 144-Rodeo de la Bordalesa, Atuel creek and Lomitas Negras-Agua del Blanco sections (Fig. 2), and they will be referred to in separate sections. A total of 25 thin sections of medium-grained sandstones were studied under the microscope and quantitatively analysed with a Swift-type point counter. Four-hundred points were counted using the traditional method of Zuffa (1984), in which grains of plutonic rock fragments are counted as such rather than as mineral components. The results were plotted in Q–F–L ternary diagrams (Dickinson & Suczek 1979; Dickinson *et al.* 1983). The populations represented in each triangle include detrital grains, with the exception of micas, opaque minerals, chlorite, heavy minerals and carbonate grains. Chert was counted as a sedimentary rock fragment.

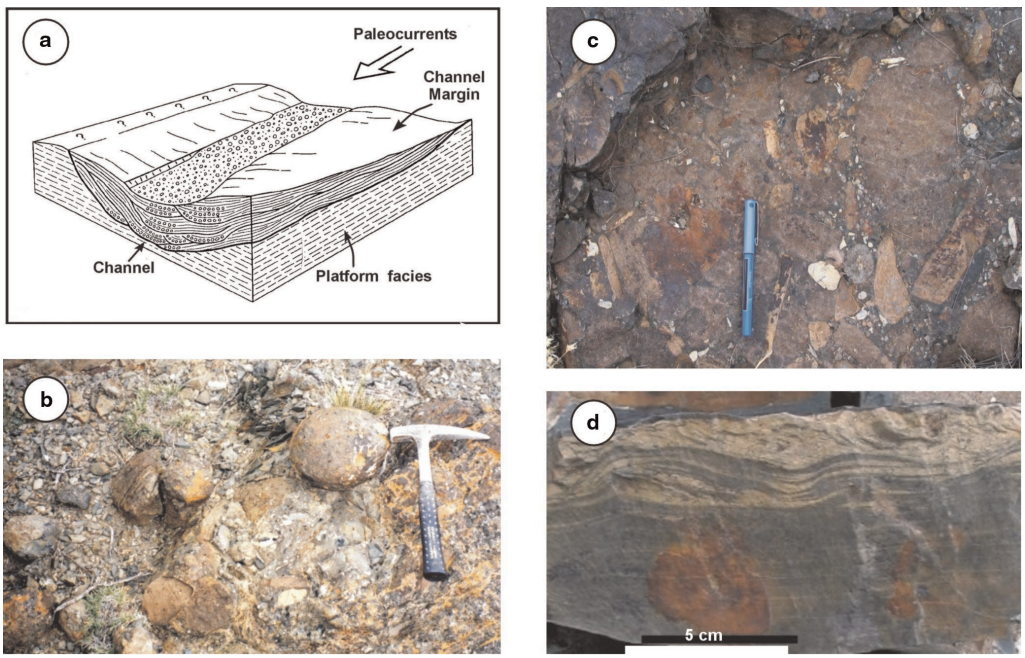

Colour online

Fig. 6. Outcrop at Lomitas Negras. (**a**) Block diagram of the conglomerate channels. (**b**) Detail of rounded clasts of the conglomerates. (**c**) Detail of subangular clasts in the conglomerates. (**d**) Syndepositional sedimentary structures showing rapid deposition in slope areas due to high water saturation.

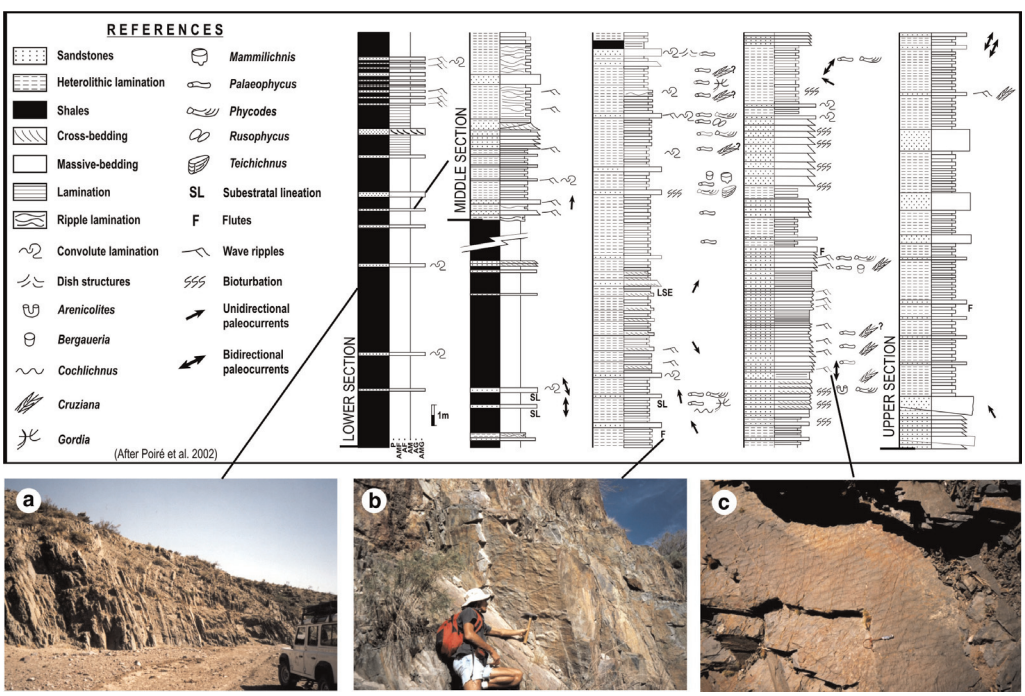

Colour online

Fig. 7. Sedimentary log at Agua del Blanco after Poiré *et al.* (2002) showing lithology, grain size, structures, trace fossils and palaeocurrents. (**a**) General view of outcrops at the base of the section with dominant heterogeneous lithofacies. (**b**) Detail of substratal structure in beds bearing trace fossils. (**c**) Wave ripples at the top of sandy beds.

Diagenesis–metamorphism studies

Diagenesis consists of a dynamic suite of processes linked to the burial history of the sedimentary basin, and the conditions which favoured different diagenetic to very low-grade metamorphic reactions are recorded in both the diagenetic fabric and mineralogy of the resulting rocks. However, the use of diagenetic features to decipher the burial history of ancient basins implies the capacity to distinguish the products of the diagenetic reactions, which characterized the different regimes at various points in the basin's history. The objective of this study was to determine the degree of diagenesis or very low-grade metamorphism overprinted in the Río Seco de los Castaños Formation. The less than 2 μm fraction of 12 samples was analysed using standardized X-ray diffraction (XRD) methods. Sieving and settling velocity techniques were performed for grain size analysis following cement removal (Moore & Reynolds 1989). Sample preparation was done according to Kisch (1980, 1991). Organic matter was eliminated with H_2O_2; carbonates were removed with acetic acid. The XRD analyses were sequentially conducted on air-dried samples that were exposed to ethylene-glycol vapours for 24 hours, and heated to 550 °C. Semi-quantitative estimates of relative concentrations of clay minerals were based on the peak area method. Percentage evaluation was based on peak height and area, corrected by factors depending on the crystallinity of the mineral. Analyses were carried out at the Centro de Investigaciones Geológicas (La Plata, Argentina), using a Philips PW 2233/20 diffractometer, set at 36 kV and 18 mA, CuKα radiation, Ni-filter, wavelength 1.54 Å (vertical goniometer). Samples were studied in the range from 2° to 32° 2θ at a 2° 2θ/min scanning velocity and with a time constant of 1 second. At the same time, international standards were analysed under the same procedures already explained in order to determine the illite crystallinity index. The thickness of sample material on each glass slide was controlled by weighting 0.058 grams of sample prior to its deposition on the glass slide. The illite crystallinity values were determined by measuring the full-width at the high-medium of the peak (001) on the air-dried and ethylene-glycol treated diffractograms, using Winfit software (Krumm 1994; Warr & Rice 1994). These illite crystallinity values were standardized according to the regression curve obtained with the standards ($y = 1.3877x - 0.1959$, $R^2 = 0.9316$, where R^2 is the correlation coefficient).

Geochemistry

Whole-rock geochemistry of sedimentary rocks reflects the average composition of the crust that shed detritus into a certain basin (Taylor & McLennan 1985). Therefore, the characteristics and location of the source area(s) can be recognized in the ultimate composition of the sedimentary succession (McLennan & Taylor 1991). However, weathering, hydraulic sorting and diagenesis acting from initial erosion of a source rock(s) to the final burial of its detritus may modify the signatures of the source rock(s), and therefore these factors need to be evaluated in order to constrain the provenance of a sedimentary sequence (Nesbitt & Young 1982; Nesbitt *et al.* 1996). Fourteen pulp samples were prepared and analysed at ACME Labs, Canada. Major elements were obtained by inductively coupled plasma element spectroscopy (ICP-ES) on fusion beads (using $LiBO_2/Li_2B_4O_7$). The loss on ignition (LOI) was calculated by weight after ignition at 1000 °C. Mo, Cu, Pb, Zn, Ni, As, Cd, Sb, Bi, Ag, Au, Hg, Tl and Se were analysed by inductively coupled plasma mass spectroscopy (ICP-MS) after leaching each sample with 3 ml 2:2:2 $HCl–HNO_3–H_2O$ at 95 °C for one hour and later diluted to 10 ml. Rare earth elements (REE) and certain trace elements (Ba, Be, Co, Cs, Ga, Hf, Nb, Rb, Sn, Sr, Ta, Th, U, V, W, Zr, Y, La, Ce, Pr, Nd, Sm, Eu, Gd, Tb, Dy, Ho, Er, Tm, Yb, Lu) were analysed by ICP-MS following lithium metaborate/tetraborate fusion and nitric acid digestion.

Nd isotopes

Nd isotopes have been widely used as provenance indicators (e.g. McLennan *et al.* 1990; McLennan 1993). Nd isotopic signatures of terrigenous sedimentary rocks provide an average of the various sources from which the sediments were derived (McLennan *et al.* 1989). Since the Sm/Nd ratio is modified during processes of mantle–crust differentiation it is possible to estimate the time at which the initial magma was separated from the upper mantle, also called the depleted mantle model age or T_{DM} (DePaolo 1981). When studying sedimentary rocks, the model age should be interpreted as the model ages of those rocks that have contributed in a higher degree to the Sm–Nd relationship of that sediment. The ε_{Nd} (t) indicates the deviation of the $^{143}Nd/^{144}Nd$ value of the sample from that of the standard CHUR (chondritic uniform reservoir; DePaolo 1981). To perform Sm–Nd analyses whole-rock samples were digested in acids (HF/HNO_3) after the addition of a combined spike of $^{149}Sm/^{150}Nd$. The Sm and Nd were separated in two stages of cation exchange columns; the first step used an AG-50x-X8 resin whereas the second step used teflon columns with a HDEHPLN-B50 anion resin. Samples were dried, dissolved in H_3PO_4 0.25 N and placed on simple (for samarium)

or triple (for neodymium) Ta-Re filaments in order to quantify the elements using a thermal ionization mass spectrometer (TIMS). Sm–Nd analyses were performed using static mode on a VG sector 54 multicollector TIMS at the Laboratorio de Geología Isotópica da Universidade Federal do Rio Grande do Sul (LGI-CPGq/UFRGS), Porto Alegre, Brazil. Nd ratios were normalized to $^{146}Nd/^{144}Nd = 0.72190$ and calculated assuming $^{143}Nd/^{144}Nd_{(0)} = 0.512638$. Measurements for the La Jolla standard gave $^{143}Nd/^{144}Nd = 0.511859 \pm 0.000010$.

Results

Lithofacies analysis

The main components of shallow marine fine-grained siliciclastics are sandstones and mudstones. The conglomerates, in this case, are restricted to channel fills in certain areas of the basin. Five main lithotypes have been recognized in this platform (Table 1). In the following paragraphs, they will be described and compared with other facies schemes in order to attribute them to one or more processes of deposition (Aguirrezabala & García Mondéjar 1994; Martino & Curran 1990; Miller & Heller 1994; Melvin 1986).

Mudstones. These rocks constitute 50% to 90% of thin beds, and show greenish colours (HUE 5GY 3/2) usually with lamination to slight bioturbation commonly in repetitive sequences. Dark to light tonality changes are frequent but they are not related to textural grading. Some mudstones of this lithofacies are massive. The fine-grained sediments are the product of suspension and fallout from low-density turbidity currents (Stow & Piper 1984) deposited in low-energy conditions. The lack of tractive structures implies transport of bed load in distal areas of the platform. The dark tonality and the scarcity of organic activity suggest anoxic conditions in low-energy environments.

Heterolithics. This is a very common facies which is characterized by alternating beds of fine to very fine grey sandstones and laminated mudstones (Figs. 5 and 7). This sedimentary association comprises thin-bedded sandstones and intercalated green (HUE 5GY 5/2) mudstones, with good lateral continuity and tabular-planar beds a few centimetres thick. The sandstone/mudstone ratio is in the range of 1:2 to 1:4. The sandstones are massive but show wavy bedding structures in some cases. They exhibit sharp contacts and in many cases wave and current ripple structures (sharp rippled tops), as well as climbing ripples (Collinson & Thompson 1989). The current wave index is in the range of 13–16 (the wave ripples have an index of 3–4 and also the symmetry index is smaller than 2.2). The dominant internal structures are normal grading, and bioturbation. As shown in Figure 7, Poiré *et al.* (2002) have recognized *Arenicolites*, *Bergaueria*, *Cochlichnus*, *Cruziana*, *Gordia*, *Mammlichnis*, *Palaeophycus*, *Phycodes*, *Rusophycus* and *Teichichnus*. This facies represents a well-oxygenated environment and it is interpreted as a proximal or shallow marine platform, with dominance of a subtidal environment. The trace fossils are developed in soft substrates of moderate energy environment. The coarse sediments were carried into below-wave-base areas by storms. The finer sediments were deposited periodically due to diminished wave and storm actions.

Laminated siltstones. These rocks comprise bedded siltstones that range in thickness from several tens of centimetres to 1 m (Figs 5 and 7). They are intercalated with fine-grained sandstones with sharp contacts. Some coarser-grained beds show small-scale ripple cross-lamination. This facies represents fine-grained sediments deposited out of suspension in low-energy environments. They may also be associated to low-density gravity flows.

Sandstones. These rocks are medium-bedded grey and green sandstones (HUE 5GY 5/2). Grain sizes range from fine to medium sand. Sandstone beds are 10 to 150 cm thick, and sometimes separated by very thin (1–2 cm) dark grey mudstones. Trace fossils, such as *Cruziana*, are also found here. The sandstones are massive and have sharp contacts. Tops of beds show current and wave ripple marks (wave index 12–20) suggesting seawater depths of *c*. 20 m (Komar 1974; González Bonorino 1986). Deformational structures such as contorted beds, dish structures and scarce flute marks are present. Sedimentary structures such as hummocks and swales can be found in this facies (Walker *et al.* 1983; Cheel & Lecki 1993) suggesting rapid deposition and storm action on the platform. The presence of plant debris indicates that the continental source area was not far away (Fig. 5a, d). The massive beds are interpreted as deposited under wave and storm actions in a proximal platform, although they may also be a product of high-density gravity flows (Moulder & Alexander 2001). The erosive bases of some beds imply a high sedimentation rate. Cross-stratification, indicative of tractive currents, is very scarce within this facies. On the other hand the dominance of thin beds with fine sediments suggests the action of low-density gravity flows in the platform.

Within the last described facies a charcoal bed that might be a marker horizon was also found (Fig. 5a, b and c). It is composed of a mixture of silty-quartz, illite-kaolinite clays and amorphous

Table 1. *Schematic lithofacies description of the Río Seco de los Castaños Formation*

Facies	Contacts	Structures	Fossils trace fossils	Stiratamorphology	Interpretation
Mudstones	Sharp	Lamination-Massive	Acritarchs	Tabular planar lamination	Proximal to distal platform with wave and storm action–high density turbidite currents
Heterolithics	Sharp	Lamination Wave ripples Normal gradation	*Arenicolites Cruziana Palaeoplycus Rusophcus Rusophycus Telchichnus Gardia Phycodes*	Tabular planar	Shallow deposits in subtidal environments of low energy
Sandstones	Sharp	Massive Wave ripples Flute marks Convolute lamination Hummocks and swaleys	Palaeophycus plant debris charcoal bed acritarchs	Tabular planar	Suspension and fall out from low density turbidity currents in distal platform
Conglomerates	Erosive Base	Poor imbrication Two modal grain sizes	Limestone clasts with Ordovician fossils	Channels	Channels perpendicular to the coast with continuity along low angle platform
Laminated Siltstones	Sharp	Bedding	–	Tabular planar	Low energy enviroments

organic matter with total organic carbon of 1%. This bed is restricted to the Atuel creek section, where it is associated with beds bearing small plant debris (Morel *et al.* 2006). Transgressive sequences have been documented widely in the sedimentary record (Collinson 1968, 1978; Reading 1996). Wave-dominated deltas have facies sequences that coarsen upwards from shelf mud through silty-sand to wave- and storm-influenced sands, capped with lagoon or strand-plains where these peat beds could developed. This seems to be the case for the Atuel section (Fig. 4) where several prograding sequences with evidence for intense wave action have been described (Fig. 4b).

Conglomerates. This facies is usually restricted to channels (2 to 3 m wide and 1 m deep), which are filled with both clast- and matrix-supported conglomerates with erosive bases (Fig. 6a). They are present only in the Lomitas Negras section. The beds are usually lenticular and laterally discontinuous (Fig. 6b and c). They are poorly sorted and contain medium- to coarse-grained sandy matrix. Clasts can be rounded (Fig. 6b) or subangular (Fig. 6c) and they range from 2 to 10 cm long and show chaotic disposition without stratification. The clasts are mainly composed of mudstones, marls, limestones, siltstones, phyllites, quartz and feldspars. Some limestone clasts bear Ordovician fossils (Nuñez 1976; Criado Roque & Ibañez 1979). In some cases, the channels show normal grading, resulting from rapid settling of gravel in high-density gravity flows (Camacho *et al.* 2002) as shown in Figure 6d. At the base of each sequence, the channels tend to be more restricted and the conglomerates are better sorted. Channels are up to several metres wide at their tops and 2 or 3 m deep. The conglomerates tend to have a subvertical position due to the regional folding of the sequence. As they are harder than the associated fine- to medium-grained sedimentary rocks, they form small hills, which is probably the main reason for the name 'Lomitas' (small hills). This facies is interpreted as channels developed perpendicular to the coast. They not only transported a coarse bed load composed of allochthonous materials (removed from the coast by wave and storm action), but by-passed them to the west into deeper sectors of the platform. The thickness of sandstones and mudstones associated with this facies suggests a high-energy environment, combined with relative instability of the coastline and close continental source areas.

Sandstone petrography.

Petrographical analyses of sedimentary rocks have proved useful for determining provenance (Dickinson *et al.* 1983), but the resolution can be enhanced by the addition of geochemistry of minor and trace elements, considering that only the more stable minerals are preserved through weathering and diagenesis. Critical analysis of the results helps to reach new conclusions about the provenance variations. The minerals recorded by point counting are quartz (monocrystalline, polycrystalline and metamorphic), K-feldspar (microcline), plagioclase, opaque minerals, hematite and sedimentary or metamorphic rock fragments. The presence of detrital biotite and scarce muscovite suggests short transport and minimal reworking of sediments. Most of the medium-grained sandstones (2 to 1.5Φ) are wackes (more than 15% matrix) and are composed of subangular quartz, with normal and wavy extinction, feldspars and fragments of polycrystalline quartz (Fig. 8). Studies using scanning electronic microscopy reveal the presence of abundant mica flakes within the framework of these sandstones (Fig. 9).

The samples from the Lomitas Negras section show higher proportions of polycrystalline quartz. The rocks are classified as feldsphathic-wackes and quartz-wackes following Dott (1964). In the Q–F–L diagrams (Figs 10 and 11), the sandstones of the Río Seco de los Castaños Formation cluster in both the recycled orogen and continental block fields. It is important to underline that the feldspars and biotite are widely altered to chlorite, giving the typical greenish colours to the rocks. In the Lomitas Negras section the abundance of polycrystalline quartz places the samples in the recycled field. Although the data show some dispersion, we could assume an uplifted igneous–metamorphic basement or recycled orogen as source areas. The facies distribution and the palaeocurrent data suggest the first option, especially when considering that outcrops of basement rocks of Mesoproterozoic age (the Cerro La Ventana Formation; Cingolani & Varela

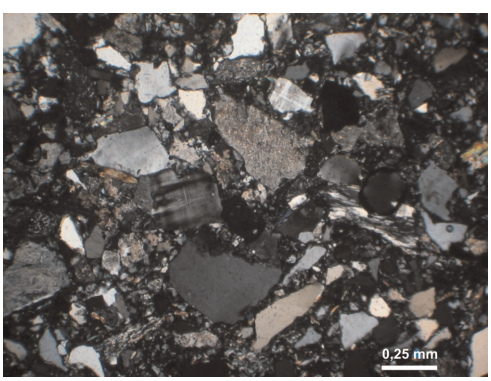

Colour online

Fig. 8. Photomicrograph of medium-grained sand and angular quartz feldspathic-wackes (crossed nicols). Note the high matrix content and subangular character of framework minerals (low textural maturity). The sample was taken from the section at Atuel creek.

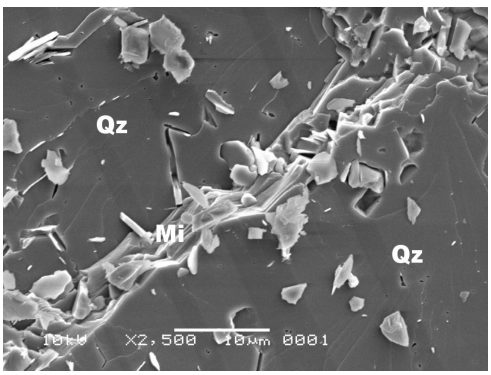

Fig. 9. Detail of Figure 8 using scanning electronic microscope, showing mica (Mi) with deformed cleavage between two quartz (Qz) crystals.

1999; Cingolani *et al.* 2005) are present to the east of the study area.

Clay composition and diagenesis

XRD analyses show that the clay mineral fraction (Fig. 12) is dominated by illite (range from 40% to 60%), followed by kaolinite (ranging from 25% to 40%), and chlorite which generally ranges from 10% to 20%, although it can rise to 35% when interlayered with smectite. Muscovite and interstratified chlorite/smectite are very scarce. Apart from the clay minerals, the fine fraction (less than 2 μm) contains very small amounts of quartz and plagioclases (see also petrographical description; chlorite may result as an alteration product of biotite). The illite crystallinity index (Fig. 13) obtained for the Río Seco de los Castaños Formation indicates that all samples were derived from the low anchizone, thus confirming that the unit suffered only a very low-grade metamorphism (Criado Roque & Ibañez 1979; González Díaz 1972). Recently, Cingolani & Varela (2007) presented the Rb–Sr isochronic whole-rock data on fine-grained samples (from the

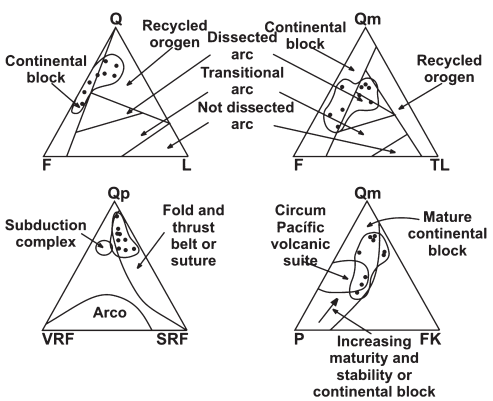

Q12 **Fig. 10.** Provenance ternary diagrams after Dickinson & Suczek (1979) and Dickinson *et al.* (1983) from sandstones from the Atuel creek section. Abbreviations: F, feldspars; FK, K-feldspars, L, lithoclasts; P, plagioclases; Q, quartz (including polycrystalline quartz); Qm, monocrystalline quartz; Qp, polycrystalline quartz.

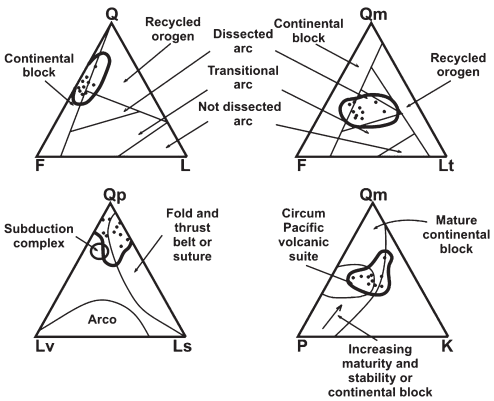

Fig. 11. Provenance ternary diagrams after Dickinson & Suczek (1979) and Dickinson *et al.* (1983) from sandstones at the Lomitas Negras section. Abbreviations: F, feldspars; K, K-feldspars, L, lithoclasts; Ls, sedimentary lithoclasts; Lt, total lithoclasts (including polycrystalline quartz); Lv, volcanic lithoclasts; P, plagioclases; Q, quartz (including polycrystalline quartz); Qm, monocrystalline quartz; Qp, polycrystalline quartz. **Q13**

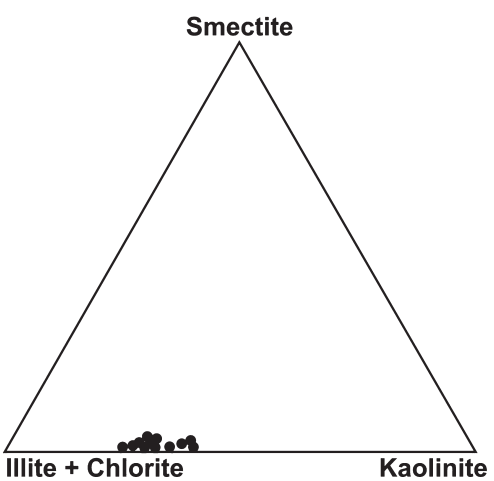

Fig. 12. Ternary diagram showing main clay composition of intercalation of claystones in the study sections. Illite and chlorite are dominant.

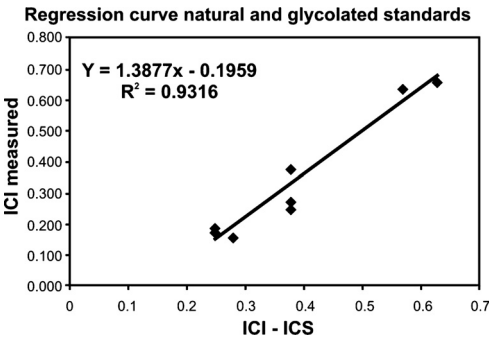

Fig. 13. Relationship between the illite crystallinity index (ICI) values of the standards as obtained at the laboratory (ICI measured) and the recommended ICI values of the standards (ICI-ICS). The regression curve obtained was used to recalculate the ICI values of all the samples in order to standardize the results and make them comparable to the worldwide established values used to separate diagenesis from very low-grade metamorphism.

Río Seco de los Castaños Formation). The obtained age was 336 $\pm$ 23 Ma with an initial $^{87}Sr/^{86}Sr$ ratio of 0.7342 and MSWD of 7.4.

Lithogeochemistry

Major elements. All the samples analysed from the Río Seco de los Castaños Formation are claystones, except for one siltstone (99S4) and one sandstone (HOR28). The differences in grain sizes explain the major element distribution (Table 2), which shows SiO_2 ranging from 52.9% to 59.9%, Al_2O_3 ranging from 18.57% to 21.4%, Fe_2O_3 concentrations between 7.68% and 9.65% and K_2O from 3.63% to 4.57% for the claystones. On the other hand, coarser fractions show SiO_2 concentrations between 70.44% and 76.82%, Al_2O_3 concentrations from 10.28% to 11.5%, Fe_2O_3 from 4.74% to 6.81%, while K_2O is between 1.41% and 1.72%. MgO and MnO concentrations as well as the LOI are lower for coarser grain-size samples. The effects of weathering on sedimentary rocks can be quantitatively assessed using the chemical index of alteration (CIA; Nesbitt & Young 1982). This index uses molecular proportions as follows: $CIA = \{Al_2O_3/(Al_2O_3 + CaO^* + Na_2O + K_2O)\} \times 100$. CaO* refers to the calcium associated with silicate minerals. Therefore, corrections for the measured CaO concentration regarding the presence of Ca in carbonates (calcite and dolomite) and phosphates (apatite) are needed. For this study, CaO was corrected for phosphate assuming that the P_2O_5 is entirely present in apatite. CIA values for the Río Seco de los Castaños Formation are between 61.1 and 78.7 (Table 2). In the A–CN–K diagram ($A = Al_2O_3$; $CN = CaO^* + Na_2O$; $K = K_2O$; Fig. 14a) the samples follow a general weathering trend which is parallel to subparallel to the A–CN join, regarding the average upper continental crust

Table 2. *Major elements (expressed in %) of the Río Seco de los Castaños Formation*

Sample	SiO_2	TiO_2	Al_2O_3	Fe_2O_3	MnO	MgO	CaO	Na_2O	K_2O	P_2O_5	LOI	SUM	CIA
Lomitas Negras and Agua del Blanco sections													
05AB1	58.47	1.03	18.62	7.68	0.08	2.92	0.48	1.49	4.00	0.18	4.80	99.75	72.05
05AB3	57.98	0.99	18.74	7.80	0.08	3.00	0.63	1.41	4.24	0.18	4.70	99.75	71.08
05AB5	55.72	1.01	19.66	8.17	0.09	3.07	1.61	1.65	4.17	0.19	4.40	99.74	66.96
05AB7	56.83	0.96	19.03	7.88	0.09	3.24	0.99	1.58	4.37	0.18	4.70	99.85	68.63
05LN2	56.65	1.01	19.88	7.97	0.08	3.17	0.46	1.57	4.34	0.19	4.40	99.72	72.18
05LN12	54.91	1.00	19.00	8.62	0.11	3.47	1.72	2.15	3.98	0.23	4.70	99.89	64.58
05LN17	56.34	0.95	19.10	8.30	0.08	3.16	0.88	1.43	4.41	0.23	5.00	99.88	70.03
05LN18	54.47	1.01	18.59	8.49	0.11	3.63	2.48	2.22	3.86	0.21	4.80	99.87	61.10
05LN22	55.45	0.96	18.57	8.88	0.10	3.83	1.21	2.16	3.72	0.23	4.80	99.89	66.79
Atuel Creek section													
05CA1	54.29	1.11	20.71	9.65	0.07	3.05	0.30	0.55	4.49	0.21	5.30	99.73	78.10
VG-2	52.94	1.14	21.41	9.17	0.07	3.14	0.25	0.88	4.57	0.14	5.00	98.71	76.67
Road 144-Rodeo de la Bordalesa section													
HOR22	59.93	1.14	19.17	8.59	0.07	1.92	0.28	0.71	3.63	0.18	3.96	99.58	78.74
HOR28	76.82	0.64	10.28	4.75	0.04	1.28	0.57	1.60	1.72	0.18	2.61	100.49	66.84
99S4	70.44	1.35	11.55	6.81	0.06	2.65	1.09	1.93	1.41	0.22	2.03	99.53	65.23
average	58.66	1.02	18.17	8.05	0.08	2.97	0.92	1.52	3.78	0.20	4.37	99.74	69.93
SD	6.47	0.15	3.07	1.14	0.02	0.64	0.63	0.50	0.95	0.02	0.90	0.36	5.07

LOI, loss on ignition (detection limit 0.1%). CIA, chemical index of alteration. SD, standard deviation. Detection limits are 0.01% for all elements, except for Fe_2O_3 which is 0.04%. Samples are claystones except for 99S4 which is a siltstone and HOR28 which is sandstone.

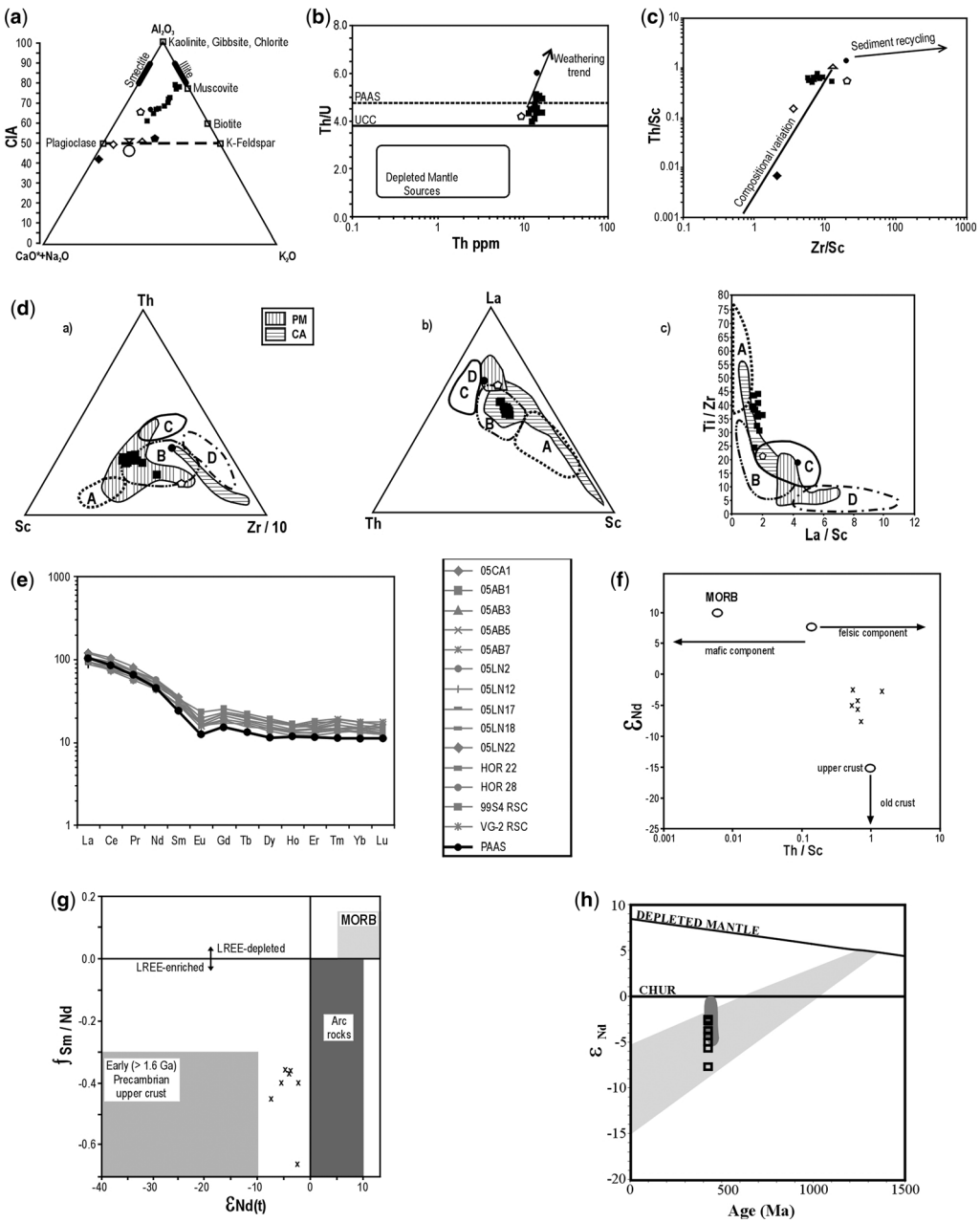

Fig. 14. Lithogeochemistry diagrams. (**a**) CIA: A–CN–K diagram constructed using molecular proportions of the oxides and with the CIA scale shown on the left. The average upper continental crust is plotted as an empty circle (Taylor & McLennan 1985), and idealized mineral compositions as empty squares. Solid pentagon, average granite; empty triangle, average adamellite; empty inverted triangle, average granodiorite; empty diamond, average tonalite; solid diamond, average gabbro (Nesbitt & Young 1989). Squares, claystones; empty pentagon, siltstone (99S4); circle, sandstone (HOR28). (**b**) Plot of Th/U versus Th (McLennan *et al.* 1993). Squares, claystones; pentagon, siltstone (99S4); circle, sandstone (HOR28). PAAS, Post-Archaean Australian Shales pattern; UCC, upper continental crust. (**c**) Th/Sc versus Zr/Sc diagram after McLennan *et al.* (1993, 2006). Empty triangle, granodiorite (average upper crust); empty diamond, andesite; solid diamond, MORB. Squares, claystones; pentagon, siltstone (99S4); circle, sandstone (HOR28). (**d**) a, Th–Sc-Zr/10; b, La–Th–Sc; c, Ti/Zr versus La/Sc discriminatory plots after Bhatia & Crook (1986). Q14

(UCC) composition (Fedo *et al.* 1995). However, deviations towards the A–K boundary are observed which could be a result of post-depositional metasomatic potassium enrichment (Nesbitt & Young 1989), as most of the samples are enriched in their K_2O concentration compared with the upper continental crust average value of 3.4% (McLennan *et al.* 2006). This metasomatism is responsible for the change of kaolinite to illite, and results in a CIA value lower than the pre-metasomatized one. It is therefore deduced that the Río Seco de los Castaños Formation is moderately to highly weathered.

Trace elements. Due to their immobile behaviour, trace elements (and in particular high field strength elements) are useful for provenance analysis because they preserve characteristics of the source rocks and therefore they reflect provenance compositions. Ratios such as Th/Sc, Th/U, Zr/Sc and Cr/V, along with the REE distribution provide some of the most useful data for provenance determination (Taylor & McLennan 1985). During weathering and/or recycling, there is a tendency for an elevation of the Th/U ratio above upper crustal igneous values of 3.8 to 4.0, because under oxidizing conditions U^{4+} oxidizes to the more soluble U^{6+} and is therefore more easily removed from the sediments than Th (McLennan 1993). Compared with Post-Archaean Australian Shale (PAAS) averages of Th (14.6 ppm) and U (3.1 ppm), most of the samples are depleted in Th and U (Table 3), although some samples are enriched in both. The Th/U ratios range from below to above the PAAS value of 4.7 but above the upper continental crust average, indicating weathering and/or recycling processes (Fig. 14b). As the CIA analysis indicates moderately to strongly weathered samples, it is deduced that weathering rather than recycling affected the samples. Another proxy to evaluate the presence or absence of recycling is the Zr/Sc ratio because Zr is strongly enriched in zircon which can be easily recycled, whereas Sc is present in labile phases (McLennan 1993). The Zr/Sc ratio for the Río Seco de los Castaños Formation (Table 3) is lower than the 13.13 value of the PAAS because Zr concentrations are lower than the PAAS average of 210 ppm and the Sc concentrations are higher than the PAAS average of 16 ppm. The exceptions are three samples which show Zr/Sc ratios between 12.75 and 21.26 due to their enrichment in Zr (HOR22 and 99S4) or depletion in Sc (HOR28) compared with the PAAS. The Th/Sc ratio indicates the degree of igneous differentiation of the source rocks since Th is an incompatible element whereas Sc is compatible in igneous systems (McLennan *et al.* 1990; McLennan 1993). The Th/Sc ratio for the Río Seco de los Castaños Formation (Table 3), except for the coarsest sample (HOR28), varies between 0.52 and 0.71, well below the PAAS value of 0.91 and the upper continental crust value of 0.79. The sandstone (HOR28) has a Th/Sc ratio of 1.4. The Zr/Sc and Th/Sc ratios indicate conclusively that for the Río Seco de los Castaños Formation recycling was not important and input was from a source geochemically less evolved than the average upper continental crust (Fig. 14c).

Cr, V, Ni and Sc are concentrated in mafic rocks, and therefore they are useful to evaluate the influence of a mafic source. The Cr/V ratio (Table 4) indicates the enrichment of Cr over other ferromagnesian trace elements. The main minerals which concentrate Cr over other ferromagnesians are chromites. The Y/Ni ratio indicates the concentration of ferromagnesian trace elements (such as Ni) compared with Y which represents a proxy for heavy REE. The Cr/V ratio is 0.79 ± 0.33 on average whereas the Y/Ni ratio is 0.86 ± 0.3 on average, plotting between the upper continental crust and the PAAS averages (diagram not shown) and indicating that although the source rock(s) was more mafic than the average upper continental crust composition, a major ophiolitic source can be ruled out. Nevertheless, the Cr/V ratio might be affected by V concentrations higher than the

Fig. 14. (*Continued*) (HOR28). (**d**) a, Th–Sc-Zr/10; b, La–Th–Sc; c, Ti/Zr versus La/Sc discriminatory plots after Bhatia & Crook (1986). A, Oceanic island arc; B, continental island arc; C, active continental margin; D, passive margin; PM, recent deep-sea turbidites derived from and deposited at a passive margin; CA, recent deep-sea turbidites derived from and deposited at a continental arc margin. The great dispersal of data showed by the PM and CA fields exemplify the difficulty of determining tectonic setting based only on geochemistry (data form McLennan *et al.* 1990). Squares, claystones; pentagon, siltstone (99S4); circle, sandstone (HOR28). (**e**) Chondrite-normalized REE patterns for the Río Seco de los Castaños Formation. PAAS pattern (Nance & Taylor, 1976) is drawn for comparison. Chondrite normalization factors are those listed by Taylor & McLennan (1985). $Eu/Eu^* = EuN/\{(SmN)(Gd_N)\}1/2$. (**f**) $\varepsilon Nd\ (t)$ versus Th/Sc ratio of samples from the Río Seco de los Castaños Formation, except sample 05LN13 for which geochemical analysis is not available. (**g**) Plots of fSm/Nd versus $\varepsilon Nd\ (t)$. fSm/Nd values for the Río Seco de los Castaños Formation are in the range of variation of the basement (see text for discussion). (**h**) Plot of εNd against age. Squares, Río Seco de los Castaños Formation; dark grey area, data from Lower Palaeozoic platform deposits from the San Rafael Block; light grey area, range of variation of εNd for the basement rocks known as Cerro La Ventana Formation. The Río Seco de los Castaños Formation Nd system can be explained mainly by the basement rocks.

Table 3. *Trace elements (expressed in ppm) of the Río Seco de los Castaños Formation*

	Lomitas Negras and Agua del Blanco sections									Atuel Creek section		Road 144-Rodeo de la Bordalesa section				
	05AB1	05AB3	05AB5	05AB7	05LN2	05LN12	05LN17	05LN18	05LN22	05CA1	VG-2	HOR22	HOR28	99S4	Aver.	SD
Mo*	0.30	0.20	0.10	0.20	0.80	0.20	0.20	0.20	0.20	0.10	bd	bd	bd	2.35	0.44	0.63
Cu*	41.50	45.40	47.50	53.50	38.20	69.10	40.80	59.50	58.85	54.7	72.19	67.03	bd	13.54	50.91	15.17
Pb*	16.30	14.60	17.70	18.40	15.30	10.90	14.90	18.10	16.90	21.5	bd	18.50	bd	bd	16.65	2.62
Zn†	86.0	87.0	94.0	97.0	97.0	88.0	97.0	97.0	101.5	106.0	33.4	120.5	bd	bd	92.0	19.82
Ni¶	46.2	41.5	41.4	44.9	45.8	42.9	44.5	45.3	47.9	50.3	63.8	41.2	bd	22.7	44.49	8.47
As‡	9.40	8.00	6.50	4.90	26.50	3.60	19.70	7.90	8.30	17.6	47.3	17.54	bd	bd	14.77	11.87
Cd*	bd	bd	0.10	0.10	0.10	0.10	bd	0.10	0.10	bd	na	na	na	na	0.10	0.00
Sb*	0.20	bd	0.10	0.10	0.20	0.10	0.10	0.20	0.10	0.10	1.69	1.82	0.33	bd	0.37	0.60
Bi*	0.40	0.40	0.50	0.50	0.40	0.30	0.40	0.60	0.60	0.50	bd	0.99	bd	bd	0.38	0.29
Ag*	bd	bd	bd	bd	bd	bd	bd	bd	bd	bd	bd	bd	bd	bd		
Au‡	bd	bd	bd	bd	0.90	1.00	bd	3.00	0.80	bd	na	na	na	na	1.43	0.91
Hg§	bd	bd	0.01	0.02	0.01	0.01	0.01	0.02	0.04	bd	na	na	na	na	0.02	0.01
Tl*	0.10	0.10	0.10	0.10	0.10	0.10	0.10	0.10	0.10	0.10	bd	bd	bd	bd	0.10	0.00
Se‡	bd	bd	bd	bd	bd	bd	bd	bd	bd	bd	na	na	na	na		
Ba†	623.8	597.3	642.8	690.7	728.6	475.6	678.9	523.7	622.5	692.3	884.8	294.8	576.3	377.4	600.6	143.4
Be†	3.00	2.00	2.00	3.00	3.00	2.00	2.00	3.00	3.00	3.0	na	na	na	na	2.60	0.49
Co^	25.20	17.60	19.10	22.10	14.80	21.60	16.40	24.60	20.65	19.4	33.55	28.04	16.77	18.85	21.33	4.91
Cr~	102.6	102.6	109.5	109.5	123.2	88.9	109.5	116.3	112.9	116.3	149.5	100.3	103.7	247.5	150.2	59.4
Cs*	10.60	11.50	9.70	10.00	9.20	8.60	10.20	8.30	9.45	13.2	9.19	5.25	6.85	3.48	8.97	2.38
Ga‡	23.20	23.60	24.70	26.60	25.20	23.20	25.30	25.00	24.55	27.3	30.16	17.16	17.16	11.03	23.16	4.73
Hf*	6.00	5.50	5.10	5.20	4.70	4.80	4.50	4.20	4.15	5.6	5.05	7.37	5.83	9.78	5.56	1.42
Nb*	18.20	17.40	17.60	17.30	16.70	16.70	16.70	16.70	16.20	19.6	23.65	15.18	13.61	14.66	17.16	2.30
Rb*	176.4	174.7	179.1	186.8	186.9	183.4	197.0	182.0	170.6	189.8	219.0	105.1	174.7	57.5	170.2	39.1
Sn†	3.00	3.00	4.00	3.00	8.00	3.00	5.00	4.00	3.00	3.0	5.34	2.24	1.83	1.07	3.53	1.65
Sr‡	77.30	56.0	120.90	72.60	102.40	114.20	61.70	153.50	75.45	47.5	77.45	50.42	93.60	97.66	85.76	28.92
Ta*	1.40	1.40	1.40	1.40	1.50	1.40	1.40	1.50	1.35	1.5	1.84	2.28	1.80	2.76	1.64	0.40
Th^	14.00	14.00	14.70	13.80	13.20	12.10	12.80	14.00	12.20	16.4	16.13	11.63	14.10	9.29	13.45	1.76
U*	3.20	2.70	2.90	2.80	3.20	2.70	2.70	3.10	3.05	3.3	3.71	2.66	2.34	2.21	2.90	0.38
V#	154.0	148.0	151.0	156.0	171.0	160.0	168.0	161.0	160.5	182.0	227.7	108.3	133.7	127.6	157.8	26.5
W‡	33.20	29.00	27.60	31.40	23.40	37.90	18.00	23.10	20.20	15.9	8.87	267.67	28.05	104.18	47.75	64.72
Sc†	22.00	22.00	23.00	22.00	23.00	23.00	22.00	23.00	22.00	23.0	26.00	22.00	10.00	18.00	21.50	3.56
Zr*	201.9	180.0	163.5	161.5	157.7	151.9	140.5	138.0	131.4	183.2	179.1	280.5	202.9	382.6	189.6	64.6
Y*	36.90	36.20	38.50	37.40	28.60	32.80	32.10	36.20	33.45	39.0	40.62	34.77	39.47	41.84	36.28	3.5

na, Not analysed; bd, below detection limit. Detection limits: *0.1 ppm; †1 ppm; ‡0.5 ppm; §0.01 ppm; ^0.2 ppm; #8 ppm; ¶20 ppm; ~0.002 ppm. Aver., average; SD, standard deviation. Samples are claystones except for 99S4 which is a siltstone and HOR28 which is sandstone.

Table 4. *Element ratios of the Río Seco de los Castaños Formation*

Sample	Lomitas Negras and Agua del Blanco sections									Atuel Creek section		Road 144-Rodeo de la Bordalesa section				
	05AB1	05AB3	05AB5	05AB7	05LN2	05LN12	05LN17	05LN18	05LN22	05CA1	VG2	HOR22	HOR28	99S4	Aver.	SD
Eu/Eu*	0.68	0.65	0.66	0.58	0.71	0.67	0.71	0.61	0.66	0.63	0.81	0.69	0.69	0.69	0.68	0.05
Ce/Ce*	0.07	0.08	0.08	0.08	0.09	0.09	0.08	0.08	0.09	0.07	0.07	0.08	0.07	0.07	0.08	0.01
Th/Sc	0.64	0.64	0.64	0.63	0.57	0.53	0.58	0.61	0.55	0.71	0.52	0.53	0.62	1.41	0.66	0.22
Zr/Sc	9.18	8.18	7.11	7.34	6.86	6.60	6.39	6.00	5.98	7.97	21.26	12.75	6.89	20.29	9.48	4.90
Th/U	4.38	5.19	5.07	4.93	4.13	4.48	4.74	4.52	4.00	4.97	4.21	4.37	4.35	6.02	4.67	0.51
Nb/Y	0.49	0.48	0.46	0.46	0.58	0.51	0.52	0.46	0.48	0.50	0.35	0.44	0.58	0.34	0.48	0.07
Ti/Zr	30.58	32.97	37.03	35.64	38.40	39.47	40.54	43.88	43.55	36.32	21.09	24.43	38.00	18.88	34.34	7.62
La/Sc	1.75	1.65	1.67	1.72	1.50	1.39	1.59	1.59	1.50	1.97	2.04	1.55	1.53	4.37	1.85	0.72
La/Th	2.76	2.60	2.62	2.75	2.61	2.64	2.73	2.61	2.70	2.77	3.96	2.94	2.47	3.10	2.80	0.35
Cr/V	0.67	0.69	0.72	0.70	0.72	0.56	0.65	0.72	0.70	0.64	1.94	0.93	0.66	0.78	0.79	0.33
La_N/Yb_N	6.59	6.56	7.07	6.65	6.84	6.04	7.19	6.56	6.63	6.99	6.22	7.10	6.16	7.46	6.72	0.40
La_N/Sm_N	3.11	3.01	3.03	3.02	3.14	3.15	3.24	3.03	2.90	3.48	2.98	3.35	3.52	3.53	3.18	0.20
Tb_N/Yb_N	1.18	1.25	1.36	1.31	1.21	1.07	1.29	1.20	1.33	1.13	1.38	1.38	1.12	1.30	1.25	0.10
Cr/Th	7.33	7.33	7.45	7.93	9.33	7.35	8.55	8.31	9.25	7.09	26.64	8.62	9.27	7.36	9.41	4.84
Zr/Th	14.42	12.86	11.12	11.70	11.95	12.55	10.98	9.86	10.77	11.17	41.17	24.11	11.10	14.40	14.87	8.04
Zr/Nb	11.09	10.34	9.29	9.34	9.44	9.10	8.41	8.26	8.11	9.35	26.09	18.48	7.57	14.92	11.41	4.97
Zr/Y	5.47	4.97	4.25	4.32	5.51	4.63	4.38	3.81	3.93	4.70	9.14	8.07	4.41	5.14	5.19	1.49
Y/Ni	0.80	0.87	0.93	0.83	0.62	0.76	0.72	0.80	0.70	0.78	1.84	0.84	0.64		0.86	0.30
Sc/Th	1.57	1.57	1.56	1.59	1.74	1.90	1.72	1.64	1.80	1.40	1.94	1.89	1.61	0.71	1.62	0.29
Gd_N/Yb_N	1.30	1.32	1.48	1.37	1.24	1.29	1.39	1.39	1.36	1.25	1.58	1.62	1.26	1.48	1.38	0.11

See text for more details. Aver., average; SD, standard deviation. Subscript N denotes chondrite normalized values. $Eu/Eu^* = Eu_N/\{(Sm_N)(Gd_N)\}^{1/2}$. $Ce/Ce^* = Ce_N/\{(0.66La_N)(0.33Nd_N)\}$. Samples are claystones except for 99S4 which is a siltstone and HOR28 which is sandstone.

PAAS value (150 ppm) since V could have been fractionated from Cr during sedimentary processes such as diagenesis (Feng & Kerrich 1990). The high Cr concentration of sample 99S4 (247 ppm), which is well above the 110 ppm average value of the PAAS, suggests the presence of chromites, which could have been derived from a mafic source, or could have been reworked (chromites are resistant heavy minerals). Nevertheless, a Zr/Sc ratio of about 20 for sample 99S4 does not suggest significant reworking.

REE pattern. The shape of the REE pattern (including the presence or absence of an Eu. anomaly) can provide information about both bulk compositions of the provenance and the nature of the dominant igneous process affecting the provenance (McLennan *et al.* 1990; McLennan & Taylor 1991). The chondrite-normalized REE diagram for the Río Seco de los Castaños Formation shows a moderately enriched light rare earth element (LREE) pattern, a negative Eu anomaly and a rather flat heavy rare earth elements (HREE) distribution (Fig. 14e and Table 5), being therefore essentially similar to the PAAS pattern. However, samples from the Río Seco de los Castaños Formation are enriched in the sum of REE compared with the PAAS, with concentrations of the elements between La and Nd varying from enriched to slightly depleted, but strongly enriched in elements between Sm and Lu. The Eu anomalies vary between 0.58 and 0.81 with an average value of 0.68, being in general higher than the average Eu anomaly for the PAAS (0.66) and for the upper continental crust (0.63). It is noteworthy that the sample with the highest Cr concentration (sample 99S4) displays a less negative Eu anomaly and the highest Eu concentration (Eu is almost double compared with the average value of the PAAS), supporting the influence of a depleted source. Sm/Nd ratios are in the range between 0.19 and 0.22, slightly higher than the average value for the PAAS (0.175).

Relationships between Th, Sc and Zr and La, Th and Sc can be useful to discriminate the tectonic setting of the depositional basin (Bhatia & Crook 1986). However, some dispersal of data is expected and caution on the interpretation is needed since detritus could have been transported across different tectonic settings (McLennan 1989). As shown in Figure 14d the samples plot within field B (continental arc settings); even those outside of any field show a trend towards the field of oceanic island arc setting (A). **Q6**

Sm–Nd isotopic data

The Río Seco de los Castaños Formation samples shows ε_{Nd} (t) values (where $t = 420$ Ma, the proxy age of sedimentation) ranging from -2.5 to -7.7 (average -4.5 ± 1.7), $f_{Sm/Nd}$ (the fractional deviation of the sample $^{147}Sm/^{144}Nd$ from a chondritic reference) ranges from -0.36 to -0.66

Table 5. *Rare earth elements data (expressed in ppm) of the Río Seco de los Castaños Formation*

Sample	La*	Ce*	Pr†	Nd‡	Sm§	Eu†	Gd§	Tb¶	Dy§	Ho†	Er^	Tm¶	Yb§	Lu¶	ΣREE
Lomitas Negras and Agua del Blanco sections															
05AB1	38.60	89.70	10.06	38.90	7.80	1.56	6.36	1.09	6.61	1.29	3.89	0.62	3.96	0.57	211.01
05AB3	36.40	85.10	9.62	34.60	7.60	1.46	6.13	1.10	6.28	1.24	3.50	0.53	3.75	0.56	197.87
05AB5	38.50	86.80	9.76	36.30	8.00	1.59	6.72	1.17	6.81	1.38	3.78	0.59	3.68	0.63	205.71
05AB7	37.90	86.50	9.82	35.80	7.90	1.37	6.50	1.18	6.74	1.38	3.86	0.59	3.85	0.58	203.97
05LN2	34.40	78.70	8.89	33.50	6.90	1.40	5.21	0.96	5.28	1.03	3.04	0.47	3.40	0.48	183.66
05LN12	32.00	71.60	8.37	32.00	6.40	1.32	5.70	0.90	5.47	1.12	3.26	0.53	3.58	0.51	172.76
05LN17	35.00	74.40	8.85	32.10	6.80	1.43	5.65	0.99	5.44	1.10	3.32	0.50	3.29	0.48	179.35
05LN18	36.60	81.50	9.37	34.40	7.60	1.40	6.47	1.06	6.33	1.19	3.65	0.58	3.77	0.53	194.45
05LN22	32.95	74.65	8.54	33.30	7.15	1.38	5.65	1.05	5.98	1.13	3.16	0.52	3.36	0.49	179.30
Atuel Creek Section															
05CA1	45.40	102.50	11.23	40.70	8.20	1.53	6.78	1.16	6.99	1.37	4.01	0.67	4.39	0.62	235.55
VG-2	39.87	83.02	9.18	36.61	7.13	1.58	6.83	1.15	6.84	1.43	4.56	0.69	4.38	0.67	203.94
Road 144-Rodeo de la Bordalesa section															
HOR22	34.21	69.86	7.72	31.26	6.43	1.47	6.50	1.05	5.84	1.15	3.57	0.53	3.26	0.48	173.33
HOR28	43.70	93.35	10.13	40.05	7.80	1.70	7.22	1.21	6.71	1.35	4.34	0.64	3.96	0.60	222.77
99S4	36.80	77.70	8.90	37.44	7.77	2.06	7.78	1.29	7.24	1.41	4.39	0.63	4.00	0.58	198.00
average	37.31	82.53	9.32	35.50	7.39	1.52	6.39	1.10	6.33	1.26	3.74	0.58	3.76	0.56	197.26
SD	3.67	8.68	0.85	2.90	0.57	0.18	0.66	0.10	0.61	0.13	0.45	0.06	0.35	0.06	17.88

SD, standard deviation. Detection limits: *0.1 ppm; †0.02 ppm; ‡0.3 ppm; §0.05 ppm; ¶0.01 ppm; ^0.03 ppm. Samples are claystones except for 99S4 which is a siltstone and HOR28 which is sandstone.

Q15 Table 6. *Sm–Nd data of the Río Seco de los Castaños Formation*

Sample	Age (Ma)	Sm (ppm)	Nd (ppm)	$^{147}Sm/^{144}Nd$	$^{143}Nd/^{144}Nd$	Error (ppm)	ε_{Nd} (0)	ε_{Nd} (t)	$^{143}Nd/^{144}Nd$ (t)	T_{DM}^{1} (Ma)	T_{DM}^{2} (Ma)	$f_{Sm/Nd}$
Lomitas Negras and Agua del Blanco sections												
05LN13	420	6.34	30.63	0.12511	0.512240	9	−7.7	−3.8	0.511900	1366	1466	−0.36
05AB7	420	7.09	34.59	0.12393	0.512220	9	−8.1	−4.2	0.511883	1381	1490	−0.37
Atuel Creek section												
05CA1	420	3.96	21.97	0.10901	0.512000	9	−12.4	−7.7	0.511705	1494	1742	−0.45
VG-2	420	5.33	27.16	0.11860	0.512130	15	−9.9	−5.7	0.511804	1448	1604	−0.40
Road 144-Rodeo de la Bordalesa section												
HOR22	420	6.14	31.70	0.11710	0.512291	110	−6.8	−2.5	0.511969	1195	1363	−0.40
HOR28	420	4.31	39.02	0.06670	0.512144	70	−9.6	−2.7	0.511960	952	1376	−0.66
99S4	420	5.40	26.12	0.12500	0.512187	57	−8.8	−5.0	0.511843	1454	1549	−0.36

$f_{Sm/Nd} = (^{147}Sm/^{144}Nd)_{sample} / (^{147}Sm/^{144}Nd)_{CHUR} - 1$. $\varepsilon_{Nd}(0) = \{[(^{143}Nd/^{144}Nd)_{sample\ (t=0)} / 0.512638] - 1\} \times 10000$. $\varepsilon_{Nd}(t) = \{[(^{143}Nd/^{144}Nd)_{sample\ (t)} / (^{143}Nd/^{144}Nd)_{CHUR\ (t)}] - 1\} \times 10000$. $(^{147}Sm/^{144}Nd)_{CHUR} = 0.1967$. $(^{143}Nd/^{144}Nd)_{CHUR} = 0.512638$. t= 420 Ma. T_{DM}^{1} (model ages) were calculated based on the depleted mantle model (DePaolo 1981) whereas T_{DM}^{2} were calculated based on the three-stage model (DePaolo *et al.* 1991). Samples are claystones except for 99S4 which is a siltstone and HOR28 which is sandstone.

(average -0.43 ± 0.10) whereas the T_{DM}^{1} ages (calculated using the model of DePaolo 1981) range from 952 to 1494 Ma (average 1327 ± 178 Ma) and T_{DM}^{2} ages (calculated using the model of DePaolo *et al.* 1991) range from 1363 to 1742 Ma (average 1513 ± 123 Ma). The ε_{Nd} values for the Río Seco de los Castaños Formation are between those typical for the upper continental crust or older crust and those typical for a juvenile component (Fig. 14 g). Regarding the relationship between ε_{Nd} (t) and Th/Sc ratio (Fig. 14f), the samples display a trend where those with the less negative ε_{Nd} values show the lowest Th/Sc ratios, indicating that the more juvenile the source the more depleted its geochemical signature. The exception is sample HOR28 which shows a low negative ε_{Nd} (t) but a high Th/Sc ratio (1.4). The plot of $f_{Sm/Nd}$ against ε_{Nd} (t) shows a data cluster between fields of arc-rocks and old crust. The $f_{Sm/Nd}$ values out of the range of variation of the upper crust (-0.4 to -0.5) could be indicating Sm–Nd fractionations due to secondary processes, and are therefore suspect (McDaniel *et al.* 1994).

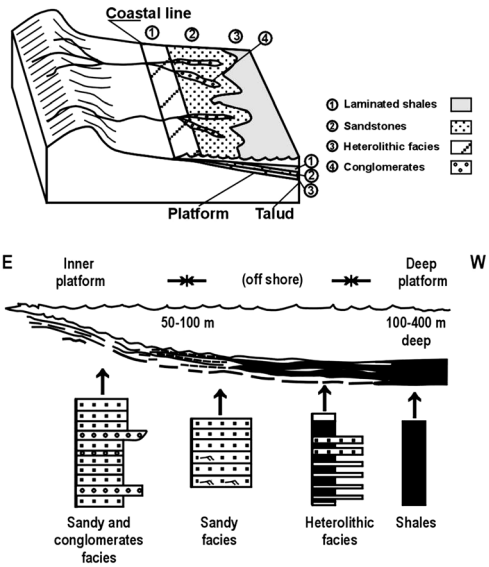

Fig. 15. Integrated block diagram showing general lithofacies distribution for the four study outcrops within the platform (adapted from Reading 1996).

Discussion and interpretation

Sedimentological studies and depositional environments

The relatively low diversity of subenvironments, dominance of fine to medium sedimentary grain sizes, lack of tractive sedimentary structures, and the significant thickness of the beds associated with gravity flow processes are typical of a distal (below wave base) to proximal marine platform-deltaic system (Fig. 15). In this case, the sedimentary input was continuous, as indicated by the absence of internal discontinuities. The basin was extended and the palaeoslope was very small (less than 1%). The dominant processes acting on this palaeoenvironment were wave and storm action, permitting the settling of fine material over the tractive processes during fairweather times. The presence of plant debris such as *Lycophytes* in the Atuel and Lomitas Negras sections suggests proximity to vegetated areas. The hydraulic regimes were moderate and the sea-level changes in this sequence generated very few sedimentary unconformities, but widespread lateral bed continuity. The ichnofacies (Poiré *et al.* 2002) such as *Cruziana* increase towards the east and the *Nereites–Mermia* towards the west of the basin which consistent with the lithofacies interpretation of deeper sectors of the basin located to the west.

Similar siliciclastic environments (probably equivalent stratigraphically), interpreted as overfilled sedimentary foreland systems with great thickness (high sedimentary rates) and low textural maturity, are found in the Villavicencio and Punta Negra formations both from the Precordillera terrane. They have been described by other authors (González Bonorino & Middleton 1976; Bustos 1996; Poiré & Morel 1996; Astini *et al.* 2005; Edwards *et al.* 2001; Peralta *et al.* 1995; Peralta 2003, 2005; Poiré *et al.* 2005). However, the channelled conglomerate and organic-matter-rich beds present in the Río Seco de los Castaños Formation, allow this unit to be distinguished from other similar environments found within the same terrane.

Diagenesis–metamorphism

The isotopic Rb–Sr ratios have been interpreted to provide the age of the low-grade metamorphism of the Río Seco de los Castaños Formation which occurred during the Late Devonian–Early Carboniferous. This metamorphic event could be linked to the final 'Chanic' tectonic phase that affected the Precordillera–Cuyania terrane (Ramos *et al.* 1986). The high Sr initial ratio suggests isotopic homogenization of the detritus which was derived from upper continental crust rocks. These Rb–Sr data also help to constrain the depositional age of the Río Seco de los Castaños Formation and the source areas.

Geochemical analyses

These data indicate moderate to strong weathering (CIA between 61 and 78 and Th/U ratios above

3.8–4), and potassium metasomatism. Zr/Sc ratios lower than 22 and no important enrichment of Zr (with some exceptions) indicate no recycling. Th/Sc ratios well below the averages for PAAS and upper continental crust, along with high Sc concentration, certain Cr enrichments and Eu anomalies less negative than PAAS and UCC, suggest a provenance from an unrecycled crust with an average composition similar to or slightly depleted compared with average upper continental crust composition. The unit seems to be related to an active margin.

Nd isotopes

T_{DM} ages are within the range of the Mesoproterozoic basement and Palaeozoic supracrustal rocks of the Precordillera terrane (Kay *et al.* 1996; Rapela *et al.* 1998; Cingolani *et al.* 2003*b*, 2005; Gleason *et al.* 2007) and the Western Pampeanas Ranges (Vujovich *et al.* 2005; Naipauer *et al.* 2005). The ε_{Nd} values of the Río Seco de los Castaños Formation are similar to those from sedimentary rocks from the Lower Palaeozoic carbonate–siliciclastic platform of the San Rafael Block, which show ε_{Nd} (t) between -0.4 and -4.9 (Cingolani *et al.* 2003*b*); they are also in the range of variation of ε_{Nd} values of the Mesoproterozoic basement of the San Rafael Block (the Cerro La Ventana Formation; Cingolani *et al.* 2005) recalculated at 420 Ma (Fig. 14 h). Although some $f_{Sm/Nd}$ values are below or above average values for the upper crust, all samples but one have $f_{Sm/Nd}$ values in the range of variation of the Cerro La Ventana Formation (Cingolani *et al.* 2005). Sample HOR28 shows a low $^{147}Sm/^{144}Nd$ ratio and a slightly negative $f_{Sm/Nd}$ value (-0.66) compared with the basement rocks, indicating that secondary processes might have fractionated Sm and Nd. Various studies have addressed processes that might alter the Sm–Nd isotopic signatures in detrital sediments. These include the alteration of Sm/Nd ratios and Nd isotopic signatures during weathering, diagenesis or sorting (McDaniel *et al.* 1994; Bock *et al.* 1994). Taking into account that sample HOR28 is a sandstone, has high Th/Sc ratios, low CIA values, and is one of the more recycled samples from this unit, it is deduced that most probably processes of sorting of LREE-enriched mineral phases might have altered its Sm–Nd isotopic signature.

In summary, the Cerro La Ventana Formation and the Ordovician carbonate–siliciclastic platform of the San Rafael Block provide a good fit to the Sm–Nd signature of the Río Seco de los Castaños Formation. Such a provenance for the Upper Silurian–Lower Devonian unit is in agreement with east to west palaeocurrents, because both sources are located to the east of the depositional basin of the Río Seco de los Castaños Formation (Fig. 16). This fact is also supported by the rather short transport deduced from the petrographical analyses (textural and compositional immaturity), as well as by the geochemical signature evidencing a non-recycled crust with an average composition similar to or depleted compared with average upper continental crust.

Provenance

A close spatial relationship between the depositional basin of the Río Seco de los Castaños Formation and the source rocks is supported by textural (e.g. subangular grains and high matrix content) and compositional (e.g. detrital mica flakes) immaturity of sandstones, the presence of plants debris and charcoal beds, and low Th/Sc ratios indicating no recycling. Petrographical analyses suggest source rocks from an igneous–metamorphic complex as well as a sedimentary source input, which included limestones bearing Ordovician fossils. Geochemical analyses and particularly the Th/Sc ratios, REE patterns and Eu anomalies further indicate that the source rocks have an average composition slightly less evolved than the average upper continental crust. The location and geochemical composition of the Mesoproterozoic basement rocks of the Cerro La Ventana Formation (igneous–metamorphic complex composed mainly of mafic to intermediate gneisses, micaschists, foliated quartz-diorites and tonalites, partially grading to amphibolites and migmatites, as well as pegmatitic and aplitic veins) and sedimentary rocks from the Ordovician carbonate–siliciclastic platform (Pavón and Ponón Trehué formations) fit the above-mentioned provenance constraints. Such a provenance location is further supported by palaeocurrents (Fig. 16). The Sm–Nd signature of the Río Seco de los Castaños Formation agrees well with the signature of both the Mesoproterozoic basement and the carbonate–siliciclastic platform (same range of variation of the ε_{Nd} (t) and T_{DM} ages), supporting such provenances (Fig. 14h).

Land–sea interactions

It is well known that the Devonian was a time of great changes not only of ecosystems but of climates as well, caused probably by complex interactions between the fast developing terrestrial biosphere, marine ecosystems and the atmosphere. The Río Seco de los Castaños Formation was deposited within a basin influenced by both terrestrial and marine environments. The continental source areas (Cerro La Ventana Formation and the Ordovician

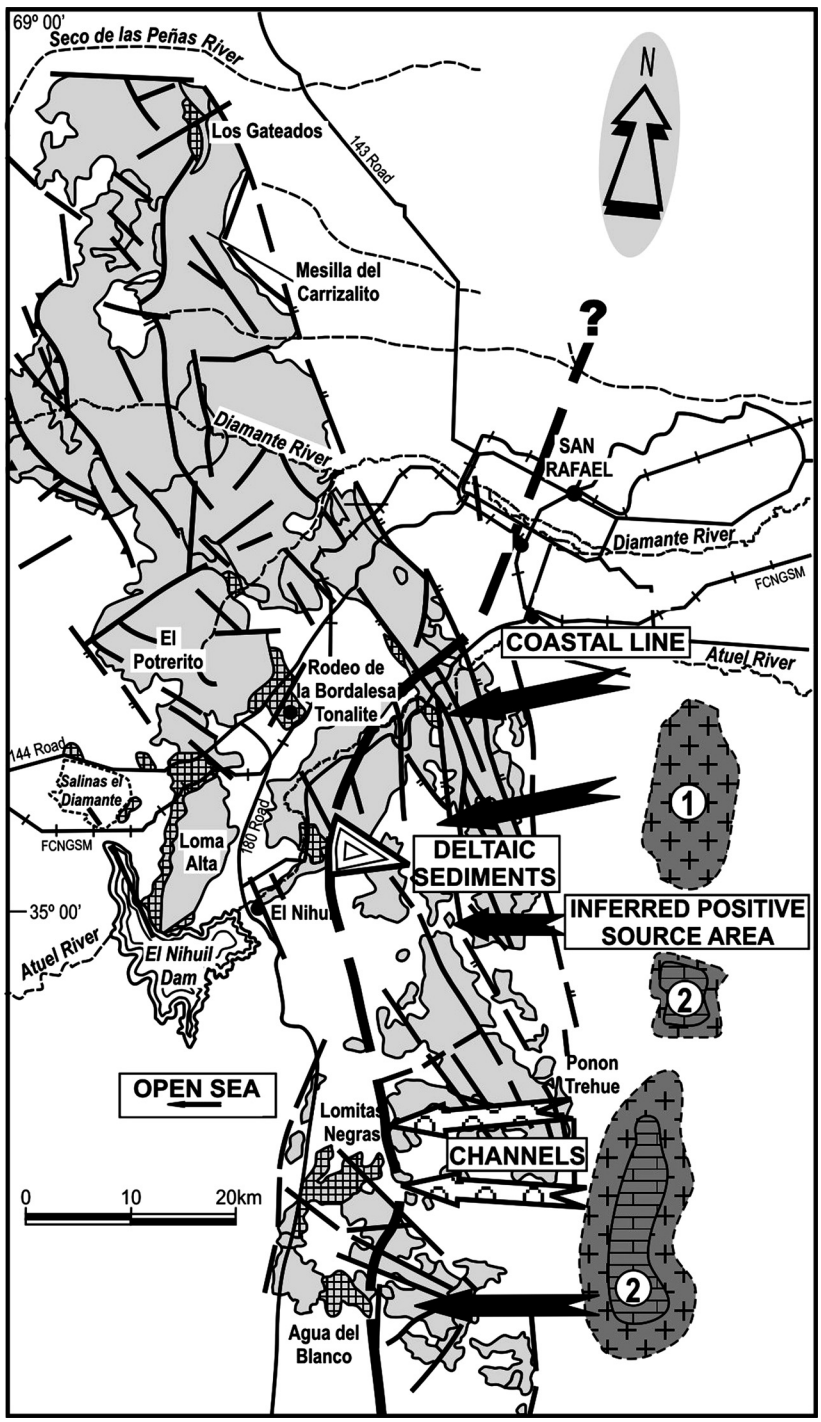

Fig. 16. Palaeogeographic interpretation. Suggested positive source areas towards the eastern side of the San Rafael Block during Upper Silurian–Lower Devonian times. key: 1, inferred location of the Mesoproterozoic crustal rocks; 2, Ordovician carbonate–siliciclastic platform (now exposed only at Ponón Trehué, see Figs 2 and 3). Interpretation of land–sea interactions: open sea towards the west of the coastal line; deltaic system and conglomerate channels on the eastern sector. For general references see Figure 2.

sedimentary units) were located not far away towards the east (Fig. 16). The detrital material was funnelled westwards (conglomerate channels) from these positive areas into the outer platform areas also laterally associated with a prograding deltaic system along coastal sectors. The basin deepened towards the west (open sea).

Conclusions

Considering the sedimentological and petrographical data, we conclude that the dominance of fine to medium grain sizes of the sedimentary rocks, lack of tractive sedimentary structures, and the important bed-thickness as well as associated gravity-flow deposition, are typical of a distal (below wave base) to proximal silty-siliciclastic marine platform-deltaic system.

The sedimentary input was continuous, as evidenced by the lateral bed continuity and absence of internal discontinuities; at the same time, the platform was extended with moderate hydraulic regimes and the palaeoslope seemed to be reduced. The dominant processes acting on the environment were wave and storm action.

The source areas were located to the east, close to the study area. The sandstone petrography shows both recycled orogen and continental block provenances. On the other hand the clay mineralogy shows that the fraction is dominated by illite (40–60%), kaolinite (25–40%) and chlorite (10–20%). The illite crystallinity index indicates very low-grade metamorphism for the sequence that occurred during the Early Carboniferous.

The presence of plant debris in the Atuel and Lomitas Negras sections suggests vegetated areas close to this Upper Silurian–Lower Devonian depocentre. Trace fossil distribution with *Cruziana* ichnofacies (indicative of a shallow environment in Agua del Blanco) to the east, and *Nereites* to the west (Road 144 outcrops) is consistent with a basin deepening towards the west.

Major element geochemistry suggests moderate to strong weathering and potassium metasomatism, in agreement with the clay mineral composition indicating an abundance of illite and kaolinite. Trace element (including REE) concentrations and ratios suggest a provenance from an unrecycled source with a composition similar to or depleted with respect to average upper continental crust.

Short transport of sediments is deduced from petrographical and sedimentological features, such as the presence of biotite and muscovite detrital flakes within sandstones, the high matrix content and subangular character of framework minerals (low textural maturity) as well as by the presence of plant debris. Facies distribution and Q–F–L diagrams indicating an uplifted igneous–metamorphic basement as source area are also in accordance with the geochemical signature. Furthermore, palaeocurrents towards the west and Sm–Nd signatures similar to those described for the Mesoproterozoic basement of the San Rafael Block (Cingolani *et al.* 2005) and the Ordovician platform, imply that the most probable sources are the Cerro La Ventana Formation and the carbonate–siliciclastic platform. The limestone conglomerate clasts also support a provenance from rocks that belong to a Lower Palaeozoic carbonate–siliciclastic platform, which is also located to the east.

A similar siliciclastic environment has been described for the Upper Silurian or Lower Devonian Villavicencio unit of the Precordillera (or Cuyania) terrane. However, the Río Seco de los Castaños Formation has two distinctive sedimentological characteristics: conglomerate channels and organic-matter-rich beds.

Continental source areas located to the east played an important role in the land–sea interactions during Upper Silurian–Lower Devonian times. The immature and poorly sorted detrital material was funnelled westwards (conglomerate channels) from these positive areas into the platform and deltaic systems. The ocean basin was open towards the west.

This contribution was supported by Argentine institution grants provided by PICT 07-10829 (ANPCYT) and PIP 5027-CONICET research projects. We are grateful to Prof. F. Chemale Jr, Prof. K. Kawashita and his technical group from UFRGS, Porto Alegre, Brazil, for the isotopic data. We thank Dr P. Könisghof (Senckenberg Museum, Germany) and Prof. M. Namik Yalçin (Istanbul University, Turkey) for the invitation to participate in this volume, for discussions and constructive comments during the field excursion and for helping us to improve this work. We sincerely acknowledge N. Uriz and E. Morel (University of La Plata, Argentina) for participation during some fieldwork. Mario Campaña is thanked for technical assistance on the paper illustrations. We are very grateful to reviewers U. Linnemann (Germany) and S. Peralta (Argentina) for their valuable comments and suggestions that deeply enhanced our manuscript in many geological and editorial aspects. Finally, we are very grateful to C. Brett (USA) for linguistic improvement of the final version. This is a contribution to IGCP 499-UNESCO-IUGS 'Devonian land–sea interaction: evolution of ecosystems and climate'.

References

ACEÑOLAZA, F. G., MILLER, H. & TOSELLI, A. 2002. Proterozoic – Early Paleozoic evolution in Western South America – a discussion. *Tectonophysics*, **354**, 121–137.

AGUIRREZABALA, L. & GARCÍA MONDÉJAR, J. 1994. A coarse turbidite system with morphotectonic control

(Middle Albian, Ondarroa, northern Iberia). *Sedimentology*, **41**, 383–407.

ASTINI, R., DÁVILA, F. *ET AL*. 2005. Cuencas de la Región Precordillerana. *In: Simposio Frontera Exploratoria de la Argentina. Congreso Exploración y Desarrollo de Hidrocarburos*, Mar del Plata, **6**, 115–145.

BHATIA, M. R. & CROOK, K. A. W. 1986. Trace element characteristics of graywackes and tectonic setting discrimination of sedimentary basins. *Contributions to Mineralogy and Petrology*, **92**, 181–193.

BOCK, B., MCLENNAN, S. M. & HANSON, G. N. 1994. Rare earth element redistribution and its effects on the neodymium isotope system in the Austin Glen Member of the Normanskill Formation, New York, USA. *Geochimica et Cosmochimica Acta*, **58**, 5245–5253.

BUSTOS, U. 1996. Modelo sedimentario alternativo para el Devónico de la Precordillera central sanjuanina: Formación Punta Negra. *Revista de la Asociación Argentina de Sedimentología*, **3**, 17–30.

CAMACHO, H., BUSBY, C. & KNELLER, B. 2002. A new depositional model for the classic turbidite locality at San Clemente State Beach, California. *Journal of American Association of Petroleum Geologists Bulletin*, **86**(9), 1543–1560.

CHEEL, R. J. & LECKIE, D. A. 1993. Hummocky cross-stratification. *In*: WRIGHT, V. P. (ed.) *Sedimentology Review*, **1**, 103–122.

CINGOLANI, C. A. & VARELA, R. 1999. The San Rafael Block, Mendoza (Argentina): Rb-Sr isotopic age of basement rocks. *II South American Symposium on Isotope Geology*, Córdoba, Actas, 23–26.

CINGOLANI, C. A. & VARELA, R. 2007. The Rb-Sr low metamorphic age of the Río Seco de los Castaños Formation, San Rafael Block, Argentina. *VI South American Symposium on Isotope Geology*, Bariloche, Argentina (in press).

CINGOLANI, C. A., BASEI, M. A. S., LLAMBÍAS, E. J., VARELA, R., CHEMALE, F. JR., SIGA, O. JR. & ABRE, P. 2003*a*. The Rodeo Bordalesa Tonalite, San Rafael Block (Argentina): Geochemical and isotopic age constraints. *10° Congreso Geológico Chileno*, Concepción (CD Rom version).

CINGOLANI, C., MANASSERO, M. & ABRE, P. 2003*b*. Composition, provenance and tectonic setting of Ordovician siliciclastic rocks in the San Rafael Block: Southern extension of the Precordillera crustal fragment, Argentina. *Journal of South American Earth Sciences* (Special Issue on the Pacific Gondwana Margin), **16**(1), 91–106.

CINGOLANI, C. A., LLAMBÍAS, E. J., BASEI, M. A. S., VARELA, R., CHEMALE, F. JR., SIGA, O. JR. & ABRE, P. 2005. Grenvillian and Famatinian-age igneous events in the San Rafael Block, Mendoza Province, Argentina: Geochemical and isotopic constraints. *Gondwana 12 Conference*, Abstracts, 102.

COLLINSON, J. D. 1968. Deltaic sedimentation units in the Upper Carboniferous of northern England. *Sedimentology*, **10**, 233–254.

COLLINSON, J. D. 1978. Vertical sequence and sand body shape in alluvial sequences. *In*: MIAL, A. D. (ed.) *Fluvial Sedimentology. Calgary*, 577–586.

COLLINSON, J. D. & THOMPSON, D. B. 1989. *Sedimentary Structures*. Unwin Hyman, London.

CRIADO ROQUE, P. & IBÁÑEZ, G. 1979. *Provincia geológica Sanrafaelino-Pampeana. In*: TURNER, J. C. (ed.) *Segundo Simposio de Geología Regional Argentina*. Academia Nacional de Ciencias, Córdoba, **I**, 837–869.

CUERDA, A. J. & CINGOLANI, C. A. 1998. El Ordovícico de la región del Cerro Bola en el Bloque de San Rafael, Mendoza: sus faunas graptolíticas. *Ameghiniana*, **35**(4), 427–448.

DEPAOLO, D. J. 1981. Neodymium isotopes in the Colorado Front Range and crust-mantle evolution in the Proterozoic. *Nature*, **291**, 193–196.

DEPAOLO, D. J., LINN, A. M. & SCHUBERT, G. 1991. The Continental Crustal Age Distribution, Methods of determining mantle separation ages from Sm-Nd isotopic data and application to the Southwestern United States. *Journal of Geophysical Research*, **96**, 2071–2088.

DESSANTI, R. 1956. *Descripción geológica de la Hoja 27c, Cerro Diamante (Provincia de Mendoza)*. Dirección Nacional de Geología y Minería, Buenos Aires, Boletín **85**.

DICKINSON, W. R. & SUCZEK, C. A. 1979. Plate tectonics and sandstone composition. *American Association of Petroleum Geologists, Bulletin*, **63**, 2164–2182.

DICKINSON, W. R., BEARD, S. *ET AL*. 1983. Provenance of North American Phanerozoic sandstones in relation to tectonic setting. *Geological Society of America Bulletin*, **64**, 233–235.

DI PERSIA, J. 1972. Breve nota sobre la edad de la denominada Serie de la Horqueta- Zona Sierra Pintada. Departamento de San Rafael, Provincia de Mendoza. *4ª Jornadas Geológicas Argentinas*, **3**, 29–41.

DOTT, R. H. 1964. Wacke, graywacke and matrix-what approach to immature sandstone classification. *Journal of Sedimentary Petrology*, **34**, 625–632.

EDWARDS, D., MOREL, E., POIRÉ, D. G. & CINGOLANI, C. A. 2001. Land plants in the Villavicencio Formation, Mendoza Province, Argentina. *Review of Paleobotany and Palynology*, **116**, 1–18.

FEDO, C. M., NESBITT, H. W. & YOUNG, G. M. 1995. Unraveling the effects of potassium metasomatism in sedimentary rocks and paleosols, with implications for paleoweathering conditions and provenance. *Geology*, **23**(10), 921–924.

FENG, R. & KERRICH, R. 1990. Geochemistry of fine-grained clastic sediments in the Archean Abitibi greenstone belt, Canada: Implications for provenance and tectonic setting. *Geochimica et Cosmochimica Acta*, **54**, 1061–1081.

FINNEY, S., GLEASON, J., GEHRELS, G., PERALTA, S. & ACEÑOLAZA, G. 2003. Early Gondwanan connection for the Argentine Precordillera terrane. *Earth and Planetary Sciences Letters*, **205**, 349–359.

GLEASON, J. D., FINNEY, S. C., PERALTA, S. H., GEHRELS, G. E. & MARSAGLIA, K. M. 2007. Zircon and whole-rock Nd-Pb isotopic provenance of Middle and Upper Ordovician siliciclastic rocks, Argentine Precordillera. *Sedimentology*, **54**(1), 107–136.

GONZÁLEZ BONORINO, G. 1986. Determinación de la profundidad de agua en que se formaron ondulitas simétricas por corrientes oscilatorias. *Primera Reunión Argentina de Sedimentología, Actas*, 221–224.

González Bonorino, G. & Middleton, G. N. 1976. A Devonian submarine fan in western Argentina. *Journal of Sedimentary Petrology*, **46**(1), 56–69.

González Díaz, E. F. 1972. *Descripción geológica de la Hoja 27d San Rafael, Mendoza*. Servicio Minero-Geológico, Buenos Aires, Boletín **132**.

González Díaz, E. F. 1981. Nuevos argumentos a favor del desdoblamiento de la denominada Serie de La Horqueta del Bloque de San Rafael, Provincia de Mendoza. *8° Congreso Geológico Argentino*, **3**, 241–256.

Kay, S. M., Orrell, S. & Abbruzzi, J. M. 1996. Zircon and whole rock Nd-Pb isotopic evidence for a Grenville age and a Laurentian origin for the basement of the Precordillera in Argentina. *Journal of Geology*, **104**, 637–648.

Kisch, H. J. 1980. Incipient metamorphism of Cambro-Silurian clastic rocks from the Jamtland Super group, Central Scandinavian Caledonides, western Sweden: Illite crystallinity and 'vitrinite' reflectance. *Journal of the Geological Society, London*, **137**, 271–288.

Kisch, H. J. 1991. Illite crystallinity: Recommendations on sample preparation, X ray diffraction settings, and interlaboratory samples. *Journal of Metamorphic Geology*, **9**, 665–670.

Krumm, S. 1994. Winfit 1.0. A computer program for X-ray diffraction line profile analysis. In XIII Conference of Clay Mineralogy and Petrology. *Acta Universitatis Carolinae Geologica*, **38**, 253–261.

Kumar, P. 1974. Oscillatory ripple marks and evaluation of ancient conditions and environments. *Journal of Sedimentary Petrology*, **44**, 169–180.

McDaniel, D. K., Hemming, S. R., McLennan, S. M. & Hanson, G. N. 1994. Petrographic, geochemical and isotopic constraints on the provenance of the Early Proterozoic Chelmsford Formation, Sudbury basin, Ontario. *Journal of Sedimentary Research*, **64**, 632–642.

McLennan, S. M. 1989. Rare earth elements in sedimentary rocks: Influence of provenance and sedimentary processes. *Mineralogical Society of America Reviews in Mineralogy*, **21**, 169–200.

McLennan, S. M. 1993. Weathering and global denudation. *Journal of Geology*, **101**, 295–303.

McLennan, S. M. & Taylor, S. R. 1991. Sedimentary rocks and crustal evolution: Tectonic setting and secular trends. *Journal of Geology*, **99**(1), 1–21.

McLennan, S. M., Taylor, S. R., McCulloch, M. T. & Maynard, J. B. 1990. Geochemical and Nd-Sr isotopic composition of deep-sea turbidites: Crustal evolution and plate tectonic associations. *Geochimica et Cosmochimica Acta*, **54**, 2015–2050.

McLennan, S. M., Taylor, S. R. & Hemming, S. R. 2006. Composition, differentiation, and evolution of continental crust: Constraints from sedimentary rocks and heat flow. *In*: Brown, M. & Rushmer, T. (eds) *Evolution and Differentiation of the Continental Crust*. Cambridge.

Manassero, M., Cingolani, C., Abre, P. & Uriz, N. 2005. Facies sedimentarias de la Formación Río Seco de los Castaños (Silúrico-Devónico) del Bloque de San Rafael, Mendoza. *XVI Congreso Geológico Argentino*, **1**, 9–16.

Martino, R. & Curran, A. 1990. Sedimentology, ichnology and paleoenvironments of the Upper Cretaceous Wenonah and Mt Laures Formations, New Jersey. *Journal of Sedimentary Petrology*, **60**(1), 125–144.

Melvin, J. 1986. Upper carboniferous fine-grained turbiditic sandstones from southwest England: A model for growth in an ancient delta-fed subsea fan. *Journal of Sedimentary Petrology*, **56**(1), 19–34.

Miller, R. & Heller, P. 1994. Depositional framework and controls on mixed carbonate-siliciclastic gravity flows: Pennsylvanian-Permian shelf to basin transect, south-western Great Basin, USA. *Sedimentology*, **41**, 1–20.

Moore, D. M. & Reynolds, R. C. 1989. *X-Ray Diffraction and the Identification Analysis of Clay Minerals*. Oxford University Press, New York.

Morel, E., Cingolani, C. A., Ganuza, D. G. & Uriz, N. J. 2006. El registro de Lycophytas primitivas en la Formación Río Seco de los Castaños, Bloque de San Rafael, Mendoza. *9° Congreso Argentino de Paleontología y Bioestratigrafía*, Córdoba. Abstract.

Moulder, T. & Alexander, J. 2001. The physical character of subaqueous sedimentary density flows and their deposits. *Sedimentology*, **48**(2), 269–299.

Naipauer, M., Cingolani, C. A., Valencio, S., Chemale, F. Jr. & Vujovich, G. I. 2005. Estudios isotópicos en carbonatos marinos del Terreno Precordillera-Cuyania: Plataforma común en el Neoproterozoico-Paleozoico inferor?. *Latin American Journal of Sedimentology and Basin Analysis*, **12**(2), 89–108.

Nance, W. B. & Taylor, S. R. 1976. Rare earth element patterns and crustal evolution I: Australian post-Archean sedimentary rocks. *Geochimica et Cosmochimica Acta*, **40**, 1539–1551.

Nesbitt, H. W. & Young, G. M. 1982. Early Proterozoic climates and plate motions inferred from major element chemistry of lutites. *Nature*, **199**, 715–717.

Nesbitt, H. W. & Young, G. M. 1989. Formation and diagenesis of weathering profiles. *Journal of Geology*, **97**, 129–147.

Nesbitt, H. W., Young, G. M., McLennan, S. M. & Keays, R. R. 1996. Effects of chemical weathering and sorting on the petrogenesis of siliciclastic sediments, with implications for provenance studies. *Journal of Geology*, **104**, 525–542.

Nuñez, E. 1976. *Descripción geológica de la Hoja Nihuil. Informe Inédito*. Servicio Geológico Nacional, Buenos Aires.

Peralta, S. 2003. An introduction to the geology of the Precordillera, Western Argentina. *In*: Peralta, S., Albanesi, G. & Ortega, G. (eds) *Ordovician and Silurian of the Precordillera, San Juan Province, Argentina*. INSUGEO, **10**, 7–22.

Peralta, S. 2005. Formación Los Sombreros: un evento diastrófico extensional del Devónico (Inferior-Medio?) en la Precordillera Argentina. *16° Congreso Geológico Argentino*, **4**, 322–326.

Peralta, S. H., León, L. I. & Carter, C. H. 1995. Estratigrafía de las sedimentitas del Eopaleozoico-Terciario de Pachaco, Precordillera Central sanjuanina. *Revista Ciencias, Facultad Ciencias Exactas, Físicas y Naturales, Universidad Nacional de San Juan*, **4**(6), 41–55.

POIRÉ, D. G. & MOREL, E. 1996. Procesos sedimentarios vinculados a la depositación de los niveles con plantas en secuencias siluro-devónicas de la Precordillera, Argentina. *VI Reunión Argentina de Sedimentología, Actas*, 205–210.

POIRÉ, D. G., CINGOLANI, C. & MOREL, E. 2002. Características sedimentológicas de la Formación Río Seco de los Castaños en el perfil de Agua del Blanco: Pre-Carbonífero del Bloque de San Rafael, Mendoza. *XV Congreso Geológico Argentino*, **I**, 129–133.

POIRÉ, D. G., EDWARDS, D., MOREL, E., BASSETT, M. G. & CINGOLANI, C. A. 2005. Depositional environments of Devonian land plants from Argentine Precordillera, South-West Gondwana. *Gondwana 12 Conference*, Mendoza. Abstract.

RAMOS, V. A. 2004. Cuyania, an exotic block to Gondwana: Review of a historical success and the present problems. *Gondwana Research*, **7**, 1009–1026.

RAMOS, V., JORDAN, T. E., ALLMENDINGER, R. W., MPODOZIS, C., KAY, S. M., CORTÉS, J. M. & PALMA, M. A. 1986. Paleozoic terranes of the central Argentine-Chilean Andes. *Tectonics*, **5**, 855–880.

RAMOS, V. A., DALLMEYER, R. & VUJOVICH, G. 1998. Time constraints on the Early Paleozoic docking of the Precordillera, central Argentina. *In*: PANKHURST, R. J. & RAPELA, C. W. (eds) *The Proto-Andean Margin of Gondwana*. Geological Society, London, Special Publications, **142**, 143–158.

RAPELA, C. W., PANKHURST, R. J., CASQUET, C., BALDO, E., SAAVEDRA, J. & GALINDO, C. 1998. Early evolution of the Proto-Andean margin of South America. *Geology*, **26**(8), 707–710.

READING, H. G. 1996. *Sedimentary Environments: Processes, Facies and Stratigraphy*. Blackwell Science, Oxford.

RUBINSTEIN, C. 1997. Primer registro de palinomorfos silúricos en la Formación La Horqueta, Bloque de San Rafael, Provincia de Mendoza, Argentina. *Ameghiniana*, **34**(2), 163–167.

SATO, A. M., TICKYJ, H., LLAMBÍAS, E. J., BASEI, M. A. S. & GONZÁLEZ, P. D. 2004. Las Matras Block, Central Argentina (37° S-67° W): The southernmost Cuyania terrane and its relationship with the Famatinian Orogeny. *Gondwana Research*, **7**(4), 1077–1087.

STOW, D. A. & PIPER, D. J. 1984. *Fine-grained Sediments: Deep Water Processes and Facies*. Geological Society, London.

TAYLOR, S. R. & MCLENNAN, S. M. 1985. *The Continental Crust: Its Composition and Evolution*. Blackwell, Oxford.

THOMAS, W. A. & ASTINI, R. A. 2003. Ordovician accretion of the Argentine Precordillera terrane to Gondwana: A review. *Journal of South American Earth Sciences*, **16**, 67–79.

TORSVIK, T. H. & COCKS, L. R. M. 2004. Earth geography from 400–250 Ma: A palaeomagnetic faunal and facies review. *Journal of the Geological Society (London)*, **161**, 555–572.

VUJOVICH, G. I., PORCHER, C., CHERNICOFF, C. J., FERNANDES, L. A. D. & PÉREZ, D. J. 2005. Extremo norte del basamento del terreno Cuyania: nuevos aportes multidisciplinarios para su identificación. *Asociación Geológica Argentina, Serie D, Publicación Especial*, **8**, 15–41.

WALKER, R. G., DUKE, W. L. & LECKIE, D. A. 1983. Hummocky cross-stratification: Significance of its variable bedding sequences, discussion. *Bulletin of the Geological Society of America*, **94**, 1245–1249.

WARR, L. N. & RICE, A. H. N. 1994. Interlaboratory standarization and calibration of clay mineral crystallinity and crystallite size data. *Journal of Metamorphic Geology*, **12**, 141–152.

ZUFFA, G. 1984. Optical analysis of arenites, influence of methodology on compositional results. *In*: *Provenance of Arenites*. Nato Series, Reidel Publishing Company, Dordrecht, 165–188.